DOE/ID/12847--4

DE93 008687

AISI DIRECT STEELMAKING PROGRAM

Annual Technical Report for Year Ending November 30, 1992

By Egil Aukrust

January 1993

Work Performed Under Contract No. FC07-90ID12847

Prepared for the
U.S. Department of Energy
Under DOE Idaho Field Office
Sponsored by the Office of the Assistant Secretary
for Conservation and Renewable Energy
Office of Industrial Technologies
Washington, D.C.

Prepared by
American Iron and Steel Institute
Washington, D.C.

ANNUAL TECHNICAL REPORT

AISI - DOE Direct Steelmaking Program

SUMMARY

The Direct Steelmaking Program has completed the fourth year of research and development since cost-share funding was provided by the Department of Energy. The program has been budgeted through Fiscal 1992 for $46,873,597, of which 77% ($36,005,587) has been funded by the federal government. Pilot plant trials with the horizontal vessel were successfully completed. The design of a third, pressurized vessel and an offgas cleaning and tempering system has been completed. Installation is now underway, with trial operation scheduled for April, 1993. A basic study and a pre-engineering design of a 350,000 metric ton per year demonstration plant have been completed, and efforts are underway to develop a program for the construction of such a demonstration plant at a host steel company that would provide the infrastructure for such a plant and a market for the product.

For this one-year reporting period, foreign filings have been prepared for the Two-Zone Countercurrent Smelter for which a U. S. patent application was prepared last year. Applications are currently being prepared for two invention disclosures submitted during the year. Six talks were given at four different conferences, and seven papers were published during the reporting year. A workshop convened at a Technical Advisory Committee meeting strongly recommended a program to explore the use of bath smelting for the recycle of steel plant waste materials.

Work by Carnegie Mellon University (CMU) and U. S. Steel with the water model of the two-zone smelter was completed. Experimental results showed that considerable backmixing takes place and that it is proportional to the total area of the holes through the barrier but independent of the number of holes. Complex concentration waves were also revealed.

The horizontal smelter program was completed. The smelter consisted of an upper, water-cooled section and a lower, refractory-lined, bathtub- shaped section. Sixteen single-zone ironmaking trials and five two-zone steelmaking trials were conducted. The first six single-zone trials with only two lances were found to be operationally unsatisfactory. The remaining 10 single-zone trials with three lances were operationally satisfactory. Early trials were conducted to evaluate equipment reliability, verify heat and mass balances, and develop process control algorithms. Postcombustion degrees of both 30% and 40% were achieved by adjustment of the lance with respect to slag foam height, and production rates in excess of 7 tph were achieved. Operating data were consistent with heat and mass balance models, with heat balance agreement generally within 5%.

Several trials were conducted to determine how sulfur is partitioned among the hot metal, the slag, and the offgas and to develop equations for predicting transient and steady-state sulfur levels. HYLSA conducted experiments with simulated reducing gas

mixtures containing sulfur and determined that the shaft furnace offgas would contain about 400 ppm H_2S when pellets alone are charged. When calcined dolomite was added to the charge, the H_2S was reduced to about 120 ppm. An H_2S scrubber system can further reduce the concentration to about 35 ppm.

For two-zone operation, a refractory dam was installed to make the ironmaking or ore-reducing side with two lances about twice the size of the steelmaking or refining side with one lance. The lance for the steelmaking side was modified to provide the projected oxygen flow rates required for decarbonization. Carbon contents of 1.0% were achieved in the steelmaking side, and the principle of carbon control by oxygen flow rate adjustment was demonstrated. The original target of 0.5% C can be achieved in a re-engineered commercial system. The results also demonstrated that for two-zone operation a dam is required; countercurrent flow alone would not provide adequate separation of zones.

Design of the offgas cleaning and tempering loop was completed by Hatch Associates, and construction and installation are now underway. A portion of the offgas from the dust-collecting cyclone will be scrubbed and cooled and recirculated with the smelter offgas to cool the stream to about 900°C to make it suitable for the cyclone and a shaft prereducing furnace that would be part of a commercial system. Dust from the cyclone is recirculated to the pressurized smelter.

Mannesmann Demag (MD) has completed the design of the pressurized vessel, and construction is underway. The working region of the vessel containing the hot metal and the foamy slag will be refractory-lined, and a transition to water-cooled staves will be made in the splash zone. Trial operation is scheduled for April, 1993. An operating program is planned through October, 1993, with the objectives of optimizing the process, perfecting the process control system, improving detection of the foamy slag level, and operating for extended periods to establish operational reliability and to reveal any unanticipated operational problems.

MD had completed a basic study of the AISI-DOE ironmaking process at the 350,000 metric ton per year level with a favorable result. A pre-engineering study of a 350,000 tpy demonstration plant has just been completed, also with a favorable result. AISI is currently preparing a proposal for such a demonstration plant, in conjunction with a host company, to be submitted to the DOE.

Laboratory research programs at CMU, McMaster University, and Praxair (formerly Linde) were conducted in support of the direct steelmaking program. CMU developed a reduction process model; studied slag foaming as a function of pressure and species of injection gas and developed an analysis of foaming based on dimensionless coefficients for use in scale-up; studied the role of sulfur in smelting, desulfurization of smelter hot metal, and rate

of removal of sulfur from the slag; and developed scale-up criteria for the smelting process.

McMaster personnel developed mathematical models of the oxygen jets and penetration of the jets into the slag and hot metal and worked with pilot plant personnel on oxygen lance design. Praxair personnel applied their parametric heat and energy balance model to the horizontal smelter; developed a quartz window system for viewing and video recording the reactions in the foamy slag; and analyzed the oxygen blowing practices and worked with pilot plant personnel on modifications to the blowing practices.

The program has been successful and will conclude with the operation of the third, pressurized vessel, coupled to the gas cleaning and tempering loop.

TASK 7 - BUDGET, PATENTS, TALKS, PUBLICATIONS, AND WORKSHOPS

Budget

The Direct Steelmaking Program has completed the fourth year of research and development since cost-share funding was provided by the DOE. The program has been budgeted through fiscal 1992 for $46,873,597, of which 77% ($36,055,587) has been funded by the federal government.

Patents

Foreign applications were filed for U. S. Patent Application Serial No. 071736,626, "Two Zone Countercurrent Smelter System."

An application is being prepared for "Fuel and Oxygen Addition for the Metal Smelting or Refining Process," Mark Schlichting, DOE Case No. S-75,841, FCH & S Case No. 1466.400400.

Disclosures have been received for "Gaseous Desulfurization in Steelmaking," Peter J. Koros, FCH & S Ref. Case No. 1466.400500, and "Method for the Direct Production of Liquid Steel," Kenneth B. Downing and Mark Schlichting, FCH & S Ref. Case No. 1466.400600.

Talks

"AISI Direct Steelmaking Project" by Egil Aukrust for the Capital Metals and Materials Forum in Washington, DC, March 26, 1992.

"Postcombustion Trials at Dofasco's KOBM Furnace" by B. L. Farrand, J. E. Wood, and F. J. Goetz for the 75th ISS-AIME Steelmaking Conference in Toronto, Ontario, April 5 - 8, 1992.

"Characterization of Oxygen Jets for Postcombustion" by Z. Du and H. Kobayashi for the 75th ISS-AIME Steelmaking Conference in Toronto, Ontario, April 5 - 8, 1992.

"Mathematical Modeling of Postcombustion in Dofasco's KOBM" by H. Gou, G. A. Irons, and W-K. Lu for the 75th ISS-AIME Steelmaking Conference in Toronto, Ontario, April 5 - 8, 1992.

"Results of the AISI/DOE Direct Steelmaking Program" by Egil Aukrust for the Savard/Lee Symposium on Bath Smelting, TMS, Montreal, Quebec, October, 1992.

"Reaction Rate and Rate Limiting Factors in Iron Bath Smelting" by R. J. Fruehan for the Savard/Lee Symposium on Bath Smelting, TMS, Montreal, Quebec, October, 1992.

"The AISI-DOE Direct Steelmaking Process - Raw Materials Requirements" by J. M. Farley and P. J. Koros for the American Mining Congress MINExpo International '92, Las Vegas, Nevada, October 21, 1992.

Publications

Sampaio, R. S., Fruehan, R. J., and Ozturk, Bahri, "Rate of Coal Devolatilization in Iron and Steelmaking Processes - Part I - Experimental Results," Transactions of ISS, August, 1992, pp. 49 - 57.

Sampaio, R. S., Fruehan, R. J., and Ozturk, Bahri, "Rate of Coal Devolatilization in Iron and Steelmaking Processes - Part II - Effect of Coal Devolatilization on Energy Efficiency in Bath Smelting," Transactions of ISS, August, 1992, pp. 59 - 66.

Ozturk, Bahri, and Fruehan, R. J., "Dissolution of Fe_2O_3 and FeO Pellets in Bath Smelting Slags," ISIJ International, Volume 32, No. 4, 1992, pp. 538 - 544.

Jiang, R., and Fruehan, R. J., "Slag Foaming in Bath Smelting," Metallurgical Transactions B, Volume 22B, August, 1992, pp. 481 - 489.

Farley, J. M., and Koros, P. J., "AISI-DOE Direct Steelmaking Program," Steel Times International, March, 1992.

Murthy, G. G. K., and Elliott, J. F., "Reduction of Fe_xO_y Pellets with Liquid Fe-C Melts and Determination of Rate Mechanisms," EPD Congress, 1992, pp. 867 - 884.

Sawada, Y., Murthy, G. G. K., and Elliott, J. F., "Reduction of FeO Dissolved in $CaO-SiO_2-Al_2O_3$ Slags by Iron-Carbon Droplets," EPD Congress, 1992, pp. 915 - 930.

Hasham, A., Pal, U. B., and Murthy, G. G. K., "Investigation of Iron Oxides Dissolved in $CaO-SiO_2-Al_2O_3$ Slags by Fe-C Melts and Determination of Rate Mechanisms," EPD Congress, 1992, ppg. 847 - 866.

Morauo, M., Murthy, G. G. K., and Elliott, J. F., "Interaction of Carbonaceous Materials with Liquid Iron-Carbon Alloys," EPD Congress, 1992, pp. 807- 820.

Workshops

The practice of establishing workshop sessions at the quarterly Technical Advisory Committee meetings to focus the attention of smaller groups on specific problems and programs has been successful. Ad hoc groups of four to eight specialists addressed such problems as carbon balance, sulfur management, future program objectives, and use of the smelter for steel plant waste material recycle. Each of the workshops provided valuable insight and guidance to the program from those with the interest and expertise to contribute the most. In particular, the steel plant waste recycle workshop was unanimous in recommending the development of a research program to explore the utility of the bath smelting process for the recycling of steel plant waste materials.

TASK 8 - PHYSICAL MODELING OF THE TWO-ZONE SMELTER

AISI has developed a two-zone horizontal smelting reactor which consists of an ironmaking zone and a steelmaking zone separated by a vertical barrier with openings in it. Carbon-saturated iron is produced in the ironmaking zone, and this flows into the steelmaking zone where it is decarbonized before tapping. The critical factor in the operation of the two zone smelter is the crossmixing flow rate between the two zones. If there were no crossmixing of metal between the two zones, the flow from the ironmaking zone to the steelmaking zone would be equal to a fraction of the production rate in the ironmaking zone. However, due to bottom gas stirring and other operating conditions, wave motions are induced in the liquid metal and, consequently, backmixing occurs. In order to understand the phenomenon of backmixing and the effect of operating parameters on it, water modeling studies were conducted on a 1/2 linear scale physical cold model.

Experimental

Figure 1 shows a schematic of the experimental set-up, and the experimental conditions are listed in Table I. Water and oil were used to simulate steel and slag, respectively. The vessel was divided into two zones separated by a physical barrier. Potassium chloride was added to either of the zones as a tracer. Conductivity probes were used to determine the change in concentration with time in both the zones. The effect of the following parameters on the backmixing rate was investigated: i) bottom blowing rate, ii) barrier design - number and area of openings, and iii) water and oil flow rates.

Results

Water modeling work revealed that the required concentration gradients between the two zones can be achieved by a simple shaped barrier. Backmixing in the water (metal) phase is proportional to the open area of the barrier and is independent of the number of the openings. The backmixing flow rate was found to be expressed by equation (1) which was obtained from the solution of dimensionless mass balance equations for the tracer.

(1)

$$Q_B = 1.85 \times 10^4 \left(\frac{S_L}{S_L - S_g}\right)^{0.4} \frac{A_o^{0.8}}{H_L^{0.2} W^{0.3}} \frac{Q_g^{0.3}}{Q_f^{0.56}} A^{1.15} S_L$$

FIGURE 1

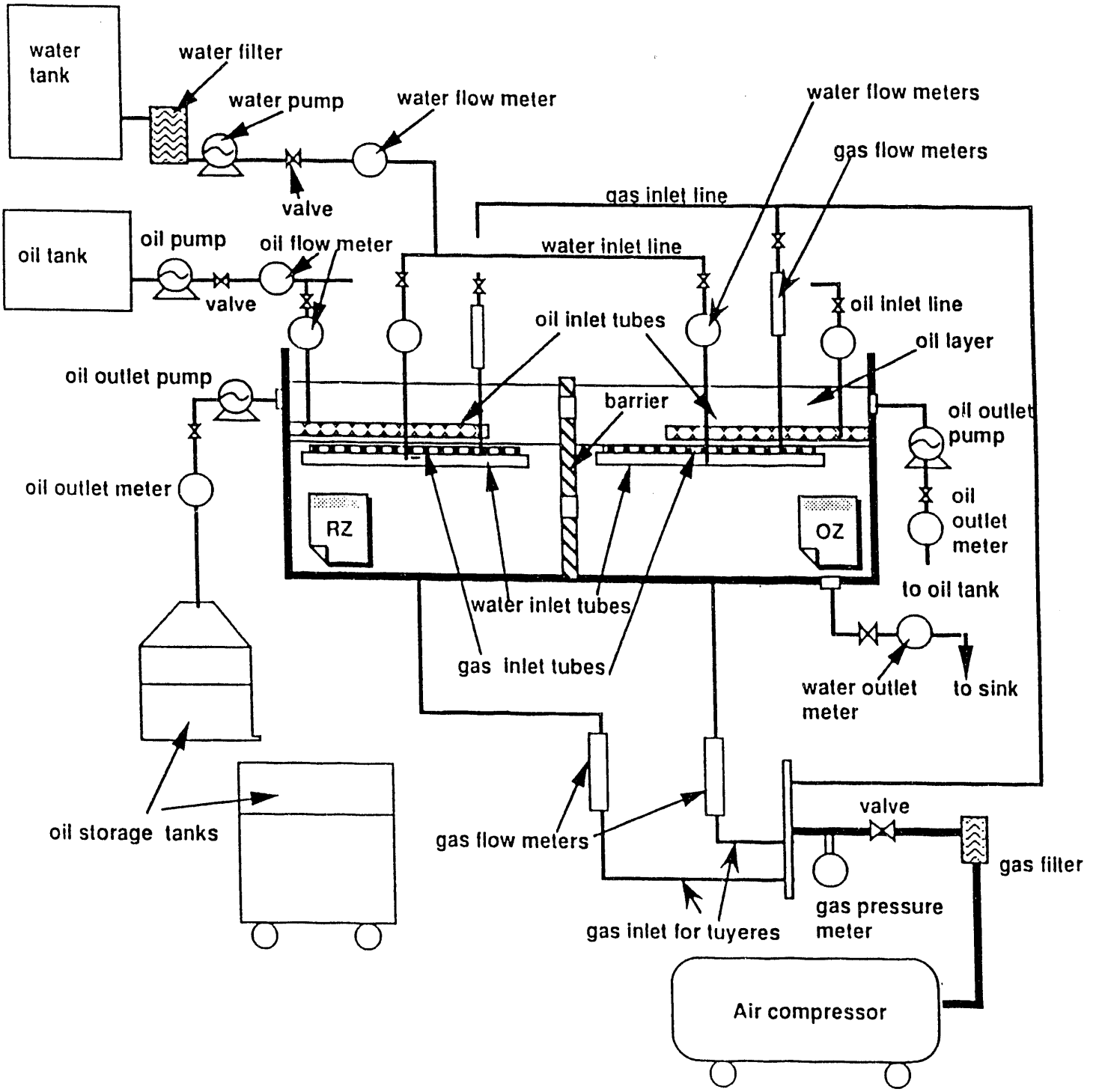

Physical model of two zone smelter

where,

Q_B - backmixing flow rate (tph)
H_L - depth of the bath (m)
W - width of the bath (m)
S_L - density of metal (kg/m^3)
S_g - density of bottom stirring gas (kg/m^3)
A - open area of the barrier (m^2)
A_o - area of the barrier in contact with metal (m^2)
Q_g - bottom gas flow rate (Nm^3/h)
Q_f - production rate in ironmaking zone (Nm^3/h)

Table I Experimental Conditions

Barrier Design	Hole type barrier (water phase); Window type barrier (water phase); 1 inch over flow barrier (oil phase); 1 inch gap barrier (oil phase)
Water flow rate total (l/min.)	2 -- 8
Bottom gas flow total rate (l/min.)	28.4 -- 311.5 (1 -- 11 scfm)
Top gas flow rate total (l/min.)	1133 -- 1700 (40 -- 60 scfm)
Oil flow rate total (l/min.)	1 -- 4
Total water volume (liters)	440
Total oil volume (liters)	62

TASK 9 - OPERATION OF THE HORIZONTAL SMELTER

Current Status

The horizontal vessel pilot plant campaign was completed in September, 1992, and work is underway to prepare the site for the third, pressurized vertical pilot smelter. Design of the offgas cooling and cleaning system is complete, and fabrication is underway. Design of the pressurized vertical vessel is complete, and specifications for the complete installation are being prepared. The schedule calls for completion of the installation and start-up and preliminary operation in April, 1993. A program for pilot plant trials through October, 1993, has been developed.

Five trials have been completed with the two-zone smelter. The basic process concept, which involves smelting in one zone and refining in the other, has been demonstrated. Carbon contents of 1 - 2% carbon have been achieved. The original target of 0.5% C can be achieved in a re-engineered commercial system.

HORIZONTAL SMELTER TEST RESULTS

Smelter Design

The horizontal smelter consisted of an upper, water-cooled section and a lower, refractory-lined section. As shown in Figure 2, the lower section was rounded at both ends and narrowed somewhat at the bottom in the cross section. Holes through the refractory were provided for charging of the vessel at the beginning of the experiments, for tapping of slag and hot metal, and for draining of slag and hot metal at the end of the experiment. The upper section was an enclosed, water-spray-cooled chamber with openings for the offgas system, material feed systems, oxygen lances, and sampling devices. The water system to the roof was equipped with flowmeters and thermocouples to accurately measure the roof heat losses. A radar slag foam height detector was installed for the last six trials. An infrared thermometer was also mounted on the roof to measure the gas temperature. A quartz window was installed for visual observation of the process.

Overview of Test Work

Twenty-one experimental trials were conducted. Table II lists the numbers of trials performed for the specified conditions:

TABLE II

Number of Trials	6	4	6	5
Number of Zones	one	one	one	two
Number of Lances	2	3	3	3
Iron Source	FeO	FeO	Fe_2O_3	Fe_2O_3/DRI

FIGURE 2

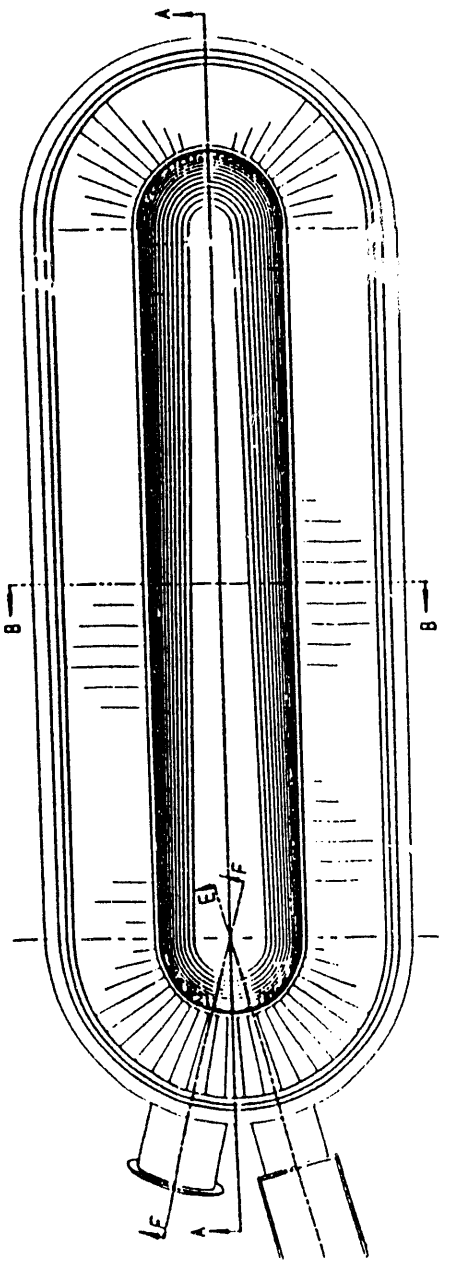

PLAN VIEW

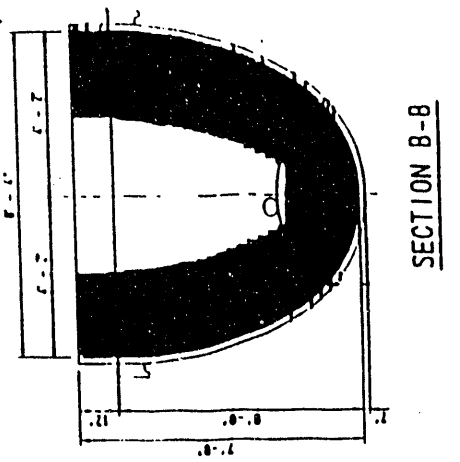

SECTION B-B

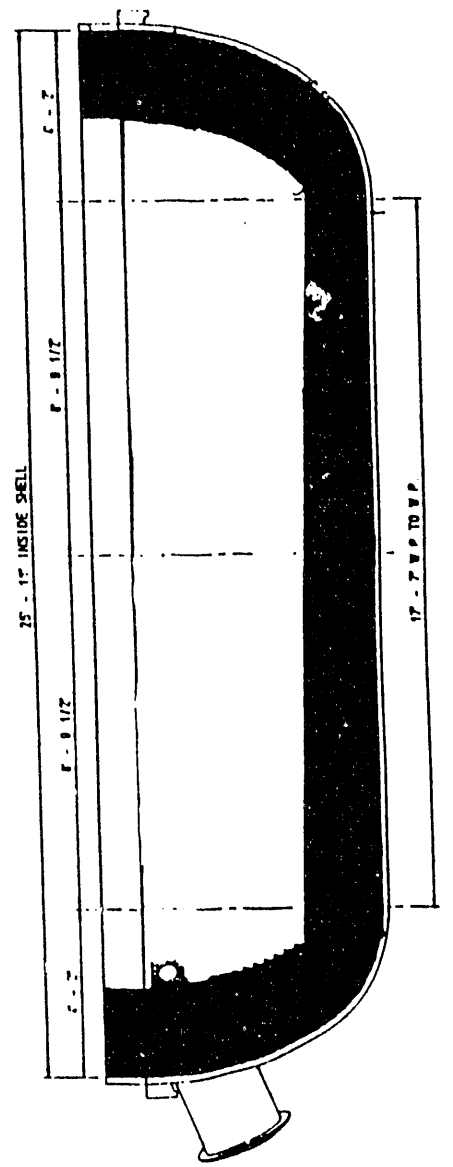

SECTION A-A

The first six trials used only two lances, which was found to be operationally unsatisfactory. The remaining fifteen trials were run with three oxygen lances in operation. Ten of those trials were run with one zone (ironmaking mode). Five trials were run with a dam installed to divide the vessel into two zones (steelmaking mode).

One Zone (Ironmaking)

The primary goals in the early ironmaking trials were to insure equipment reliability, verify heat and mass balances, and practice stable operation in preparation for the steelmaking trials. The third lance was installed after trial 6. It was difficult to achieve proper oxygen distribution and mixing at the center of the vessel, even after the installation of side air tuyeres. The problem was compounded by the raw materials entering the vessel between the lances and being moved toward the center of the vessel. The installation of the center oxygen lance solved this problem, and the process reacted in very much the same fashion as it did with the vertical vessel.

The last three trials, conducted after the steelmaking trials, focused on definition of the sulfur distribution between the hot metal, slag, dust, and offgas. Practices at both 30% and 40% PCD were established by adjustment of the lance with respect to slag foam height. Production rates in excess of 7 tph were achieved. Operating data were consistent with heat and mass balance models, with heat balance agreement generally within 5%.

Two Zone (Steelmaking)

For steelmaking experiments, the vessel was divided into two zones by installing a refractory dam (see Figure 3). Two of the oxygen lances were located in the ironmaking zone, along with the raw material feed chutes. The steelmaking zone was located at the end of the vessel directly under the offgas system. The single oxygen lance in the steelmaking zone was modified for the projected flow rates required for decarbonization. Provisions were made for manual feeding of raw materials into the steelmaking zone.

The concept was to operate each zone of the vessel relatively independently. The ironmaking zone was operated as steadily as possible, maintaining carbon saturation (excess char) and thermal control using the control strategies employed in previous experimentation. Carbon-saturated iron produced in the ironmaking zone flowed through a hole in the bottom of the dam into the steelmaking zone. There the metal was decarbonized by the oxygen lance, and low carbon metal was tapped from the steelmaking zone.

FIGURE 3

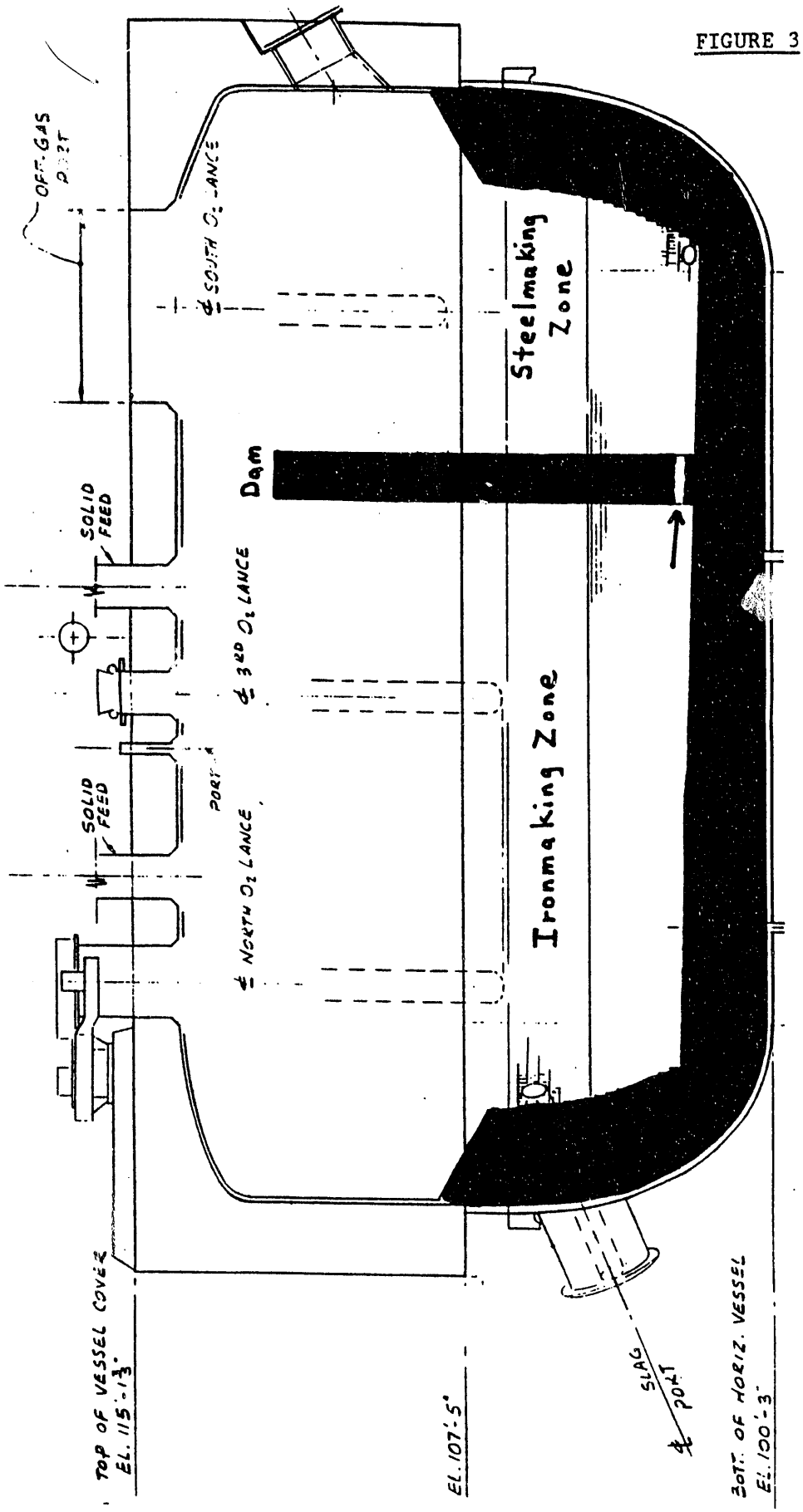
OFF-GAS PORT
℄ SOUTH O₂ LANCE
Steelmaking Zone
Dam
SOLID FEED
℄ 3RD O₂ LANCE
SOLID FEED
PORT
℄ NORTH O₂ LANCE
Ironmaking Zone
TOP OF VESSEL COVER EL. 115'-13"
EL. 107'-5"
SLAG PORT
BOTT. OF HORIZ. VESSEL EL. 100'-3"

Slag Management

Slagmaking ingredients were added to the steelmaking zone at the beginning of each experiment to establish a small slag volume with a basicity (CaO/SiO_2) of 1.6 or greater. Slag in the ironmaking zone was maintained at basicities of 1.0 to 1.2. When necessary to control the amount of slag in the ironmaking zone, slag was drained through a slag hole.

Dam Hole Size and Backmixing

The two zone configuration of the horizontal vessel involved the physical separation of the ironmaking side from the steelmaking side by a refractory dam. Hot metal produced in the iron side flowed through an opening at the bottom of the dam to the steel side where decarbonization was performed. Water modeling studies conducted by CMU and USS researchers reported under Task 8 indicated that the prevailing turbulent conditions would cause metal to flow from the steel side back to the iron side, and the rate of this backmixing or backflow was found to be proportional to the area of the opening under the dam. A knowledge of the backflow rate is required to be able to control the carbon content on the steel side.

In order to determine the backmixing rate, copper was used as a tracer and added to the steel side. Metal samples were collected from the iron and steel sides periodically and analyzed for the copper content. The rate of change of the copper content in the metal on the iron and steel sides is given by equations (2) and (3), respectively. These equations were obtained by solving the mass balance for copper.

(2)

$$\frac{dC_i}{dt} = \frac{Q_b}{(1-x)(W_{T,0}+W_P t)}\left[\frac{W_{T,0}(C_{i,0}+x(C_{s,0}-C_{i,0})) - (W_{T,0}+W_P t)C_i}{x(W_{T,0}+W_P t)} - W_P C_i\right]$$

(3)

$$\frac{dC_s}{dt} = \frac{Q_b+xW_P}{x(1-x)(W_{T,0}+W_P t)^2}[W_{T,0}(C_{i,0}+x(C_{s,0}-C_{i,0})) - (W_{T,0}+W_P t)C_s]$$

where,

Q_B = backmixing flow rate (tph)
W_P = production rate in ironmaking side (tph)
$W_{T,0}$ = initial weight of liquid metal
$C_{s,0}$ & $C_{i,0}$ = initial conc. of Cu in steel and iron sides
C_s & C_i = conc. of Cu at time t in steel and iron sides
and x = weight fraction of steel side.

Equations (2) and (3) were solved numerically to obtain the rate of backmixing from the data obtained in the copper tracer experiments. Figure 4 shows the data obtained along with the predicted concentrations (represented by lines). The dam opening was successively reduced for the next three trials to result in backflow rates of 5 tph.

In Figure 5, the backflow rate is plotted against the initial area of the opening under the dam. A linear relationship between the backflow rate and the opening area was obtained. This was consistent with the results obtained from the water model studies. Thus, based on mass balance equations and copper tracer experiments, it was possible to design the opening of the area under the dam to obtain a backflow rate of 5 tph.

Operating Practices

Coke was used with hematite and DRI to achieve high production rates with the reduced volume (about 2/3 of the vessel) of the ironmaking zone. Stable operation was achieved at 40 - 60% PCD with production rates of 7 - 9 tph.

Carbon Balance and Control

All of the elements of the carbon balance may be measured directly from operating parameters except the sum of the carbon from backmixing and from dissolution, which may be calculated by difference. By projecting the carbon from backmixing and dissolution from previous values, it may be possible to predict the expected carbon accumulation (or depletion) in the steelmaking zone. This would then serve as the basis for a carbon control strategy in which the oxygen flow rate would be adjusted to achieve the desired carbon accumulation or depletion (zero at steady state).

Application of Carbon Control Principles to Operating Data

Data from the steelmaking trials were used to evaluate the prediction of the carbon level from previous operating data. For each sample period, the carbon from backmixing and dissolution was calculated by difference. Weighted averages of the last three sample periods were used to estimate the carbon from backmixing and dissolution for the next sample period. The predicted carbon level for the end of the next sample period was then calculated from the carbon balance.

FIGURE 4

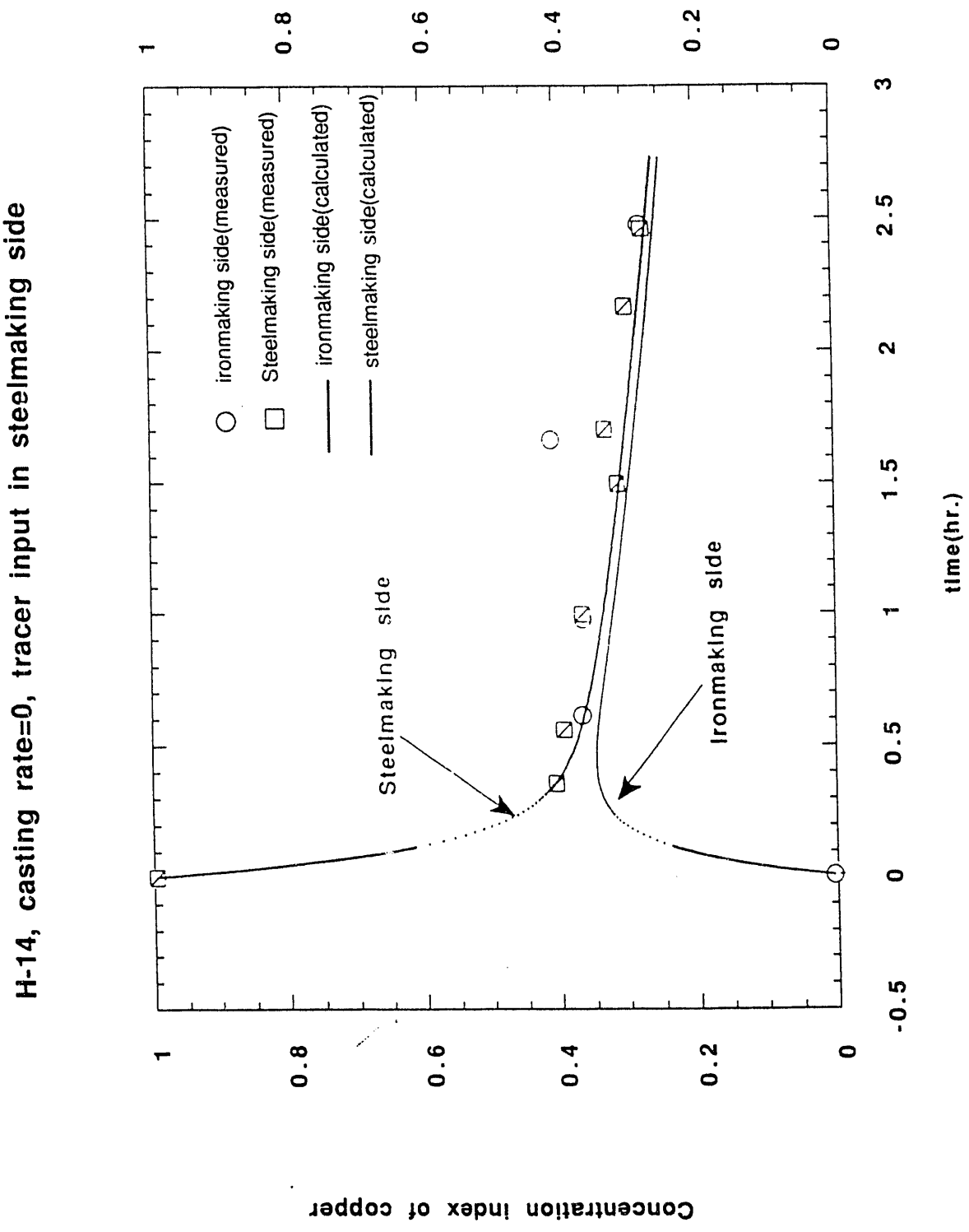
H-14, casting rate=0, tracer input in steelmaking side
Concentration index of copper
time(hr.)
ironmaking side(measured)
Steelmaking side(measured)
ironmaking side(calculated)
steelmaking side(calculated)
Steelmaking side
Ironmaking side
1
0.8
0.6
0.4
0.2
0
-0.5
0.5
1.5
2
2.5
3

FIGURE 5

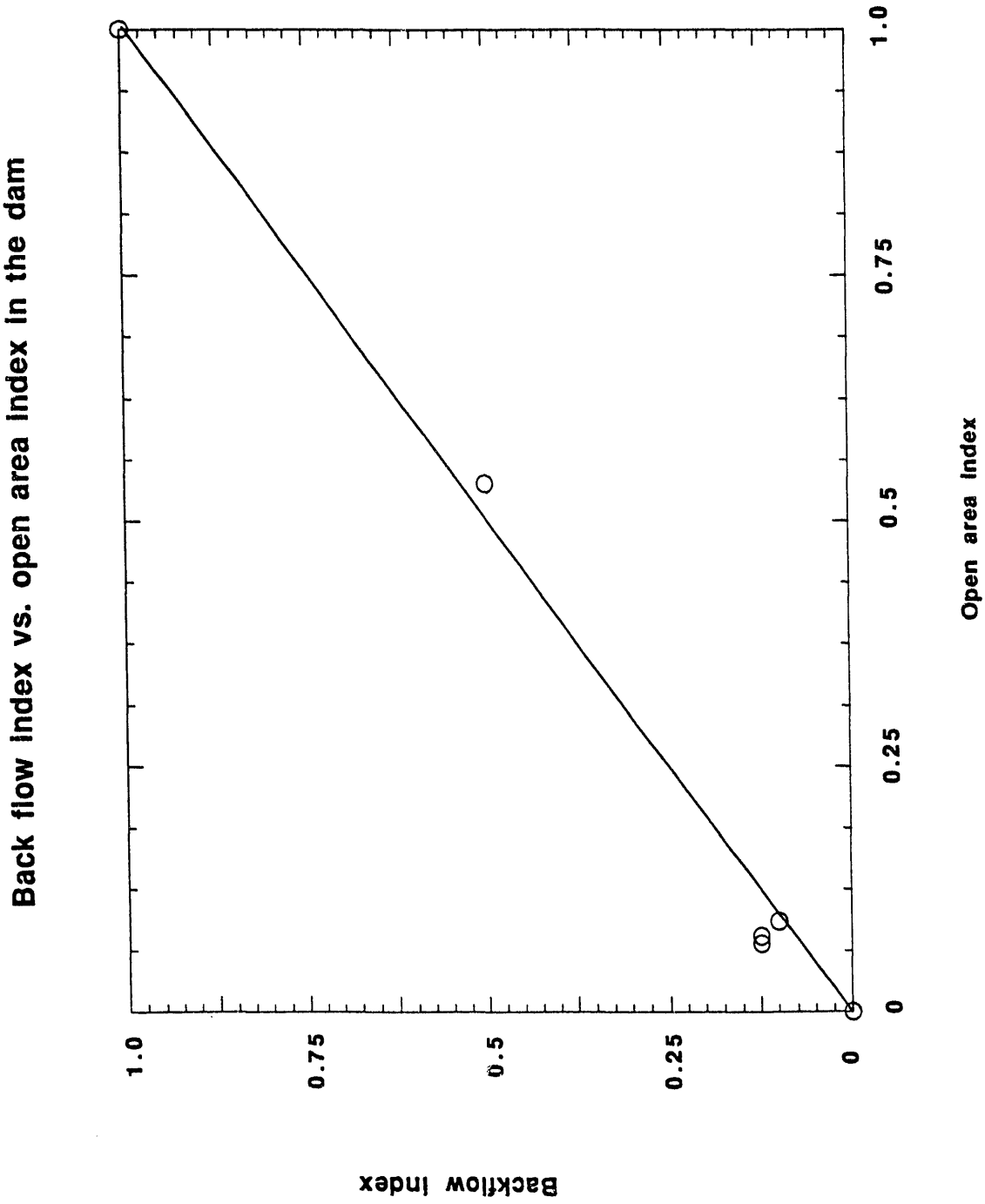
Back flow index vs. open area index in the dam
Backflow Index
1.0
0.75
0.5
0.25
0
Open area index
0
0.25
0.5
0.75
1.0

Discussion of Operating Results

During the experiments, oxygen flow rates were adjusted in increments of 100 Nm^3 to observe the effect on carbon level in the steelmaking zone. Other factors, such as variations in production, casting, backmixing, and dissolution, affected the carbon levels as described by the carbon balance. In this manner, carbon levels down to 1.0% were achieved, and the principle of carbon control by oxygen flow rate adjustment was demonstrated. Equipment and time limitations prevented extended periods of control at low carbon levels, however.

Evaluation of Vessel Design

The feasibility of producing low carbon iron in a two-zone smelter was demonstrated. It was also apparent that separation of the vessel into high and low carbon zones would be impossible without physical separation by the dam. Heat and mass balances were performed for the steelmaking zone of a 50 tph horizontal two-zone smelter operating at 1600°C and 1.0% carbon.

SULFUR MANAGEMENT

Sulfur Distribution in Slag and Hot Metal

In the smelting process, sulfur enters the system via coal and recycled materials as dust. Much of the sulfur in the coal goes into the gas phase during devolatilization and combustion, and a fraction of the total sulfur input from coal enters the slag and metal phases. Sulfur in the metal and slag is present as dissolved sulfur. However, depending on the temperature and solubility limit, second phase particles containing sulfur, such as CaS, may exist in the slag.

Assuming that all the sulfur in the slag is in solution, sulfur accumulation in the slag and the hot metal must equal the sulfur input minus the sulfur output. If sulfur removal from the slag by the slag-gas reactions is first order with respect to the sulfur content of the slag, the accumulation of sulfur in the slag and metal is given by equation 4,

$$(4)\quad \frac{W_s}{100}\frac{d(\%S)}{dt}+\frac{W_m}{100}\frac{d[\%S]}{dt}+\frac{dW_s}{dt}\frac{(\%S)}{100}+\frac{dW_m}{dt}\frac{[\%S]}{100} = \alpha F_S^C + \beta F_S^R - \frac{(\%S)}{100}k$$

where α is the fraction of sulfur from coal that enters slag and metal, F_S^C is the sulfur input from coal (kg/min), ß is the fraction of sulfur from recycled dust that enters the slag and metal, F_S^R is the sulfur input from recycled dust (kg/min), k is the rate constant for sulfur removal from slag by gas (kg/min %S), (% S) is the sulfur content of slag, W_s is the weight of slag (kg), [% S] is the sulfur content of metal, and W_m is the weight of metal (kg).

Assuming that sulfur present in the slag and metal are at equilibrium with respect to slag-metal sulfur transfer, we can define a constant partition ratio L_s = (% S)/[% S]. L_s is dependent on slag basicity, FeO content in slag, carbon content in the metal, and temperature, and may be assumed to be constant if the slag and metal chemistry do not change. Analysis of the data obtained during the vertical vessel campaign indicated that the slag-metal reaction is at equilibrium, and the oxygen potential at the slag-metal interface is controlled by the Fe-FeO reaction. Figure 6 shows the comparison between the measured sulfur partition ratio with that estimated using an approach involving optical basicity and assuming the oxygen potential is controlled by the Fe-FeO reaction. There is good agreement between the measured and predicted values, and this validates the assumption that the slag-metal reaction involving sulfur transfer is at equilibrium. Equation 4 can now be rewritten as equation 5,

$$(5) \quad \alpha F_S^C + \beta F_S^R = \frac{(\%S)}{100}\left[k + \frac{dW_s}{dt} + \frac{1}{L_S}\frac{dW_m}{dt}\right] + \frac{1}{100}\left[W_s + \frac{W_m}{L_S}\right]\frac{d(\%S)}{dt}$$

The slag weight, W_s, and the metal weight, W_m, are time dependent. For the purpose of this analysis, an average will be considered. For a given set of operating conditions, all the terms, except (%S), in equation 2 will be constant, and it may be solved for (%S) and integrated to yield equation 6,

$$(6) \quad (\%S)_t = A - [A - (\%S)_0]\, e^{-Bt}$$

$(\%S)_0$ is the sulfur content at t = 0, and the terms A and B are as defined in equations 7,

$$(7) \quad A = \frac{100(\alpha F_S^C + \beta F_S^R)}{k + \frac{dW_s}{dt} + \frac{1}{L_S}\frac{dW_m}{dt}} \quad and \quad B = \frac{k + \frac{dW_s}{dt} + \frac{1}{L_S}\frac{dW_m}{dt}}{W_s + \frac{W_m}{L_S}}$$

At steady state, the rates of change of sulfur in the slag and sulfur in the metal are zero, so the steady-state equation for the sulfur in the slag is that shown in equation 8,

$$(8) \quad (\%S)_{stst} = \frac{100(\alpha F_S^C + \beta F_S^R)}{k + \frac{dW_s}{dt} + \frac{1}{L_S}\frac{dW_m}{dt}}$$

Thus, for a given set of operating conditions, if α, ß, and k are known, the steady-state sulfur content can be evaluated. Alternatively, steady-state data from the pilot plant may be used

FIGURE 6

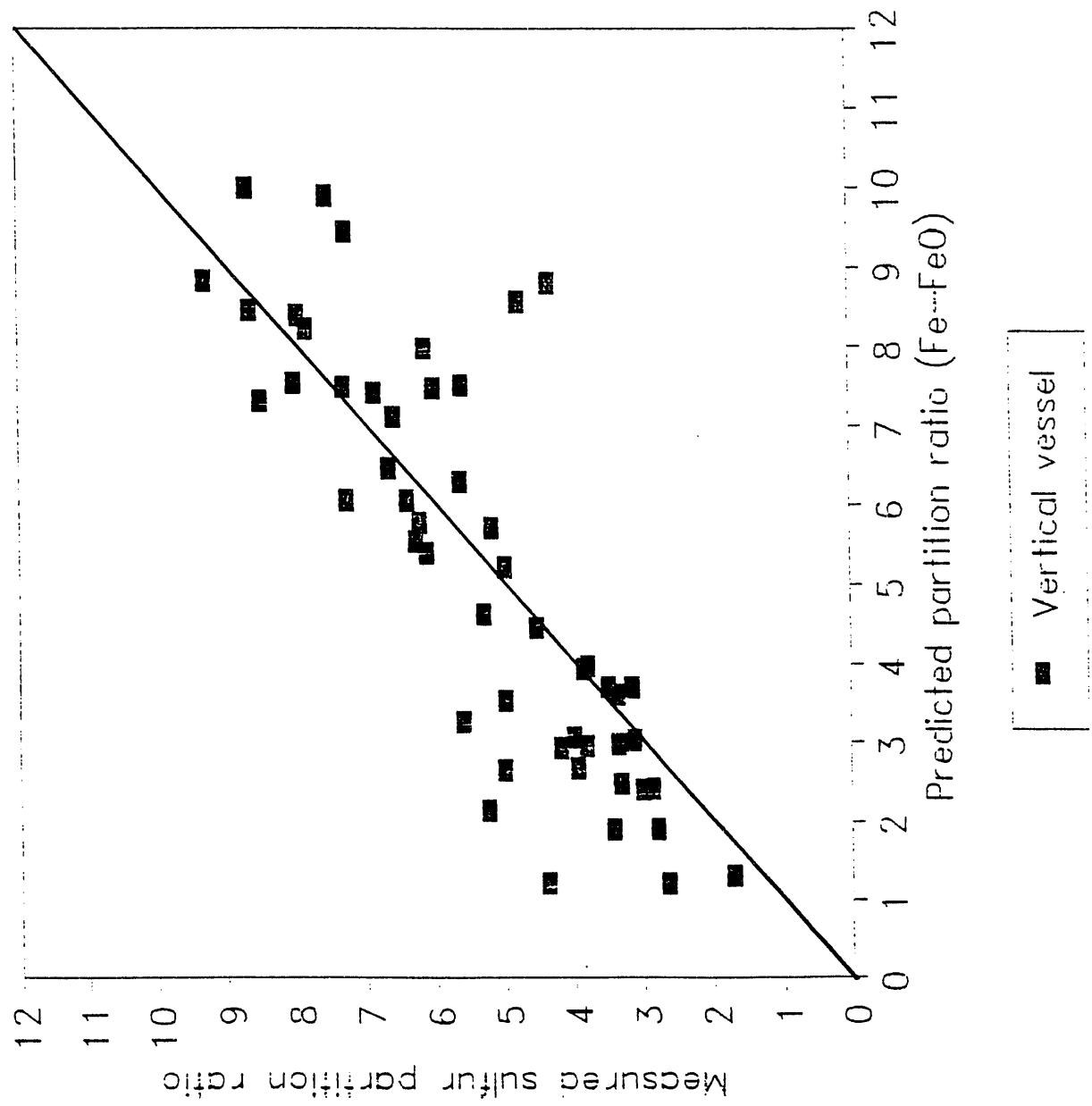

COMPARISON BETWEEN MEASURED SULFUR PARTITION RATIOS WITH THOSE PREDICTED ASSUMING THE OXYGEN POTENTIAL IS CONTROLLED BY THE Fe-FeO REACTION. DATA FROM VERTICAL VESSEL CAMPAIGN.

to determine the relationship between α and k (F_S^R = 0, since no recycled dust was used). α is expected to depend on the type of coal used and is expected to be constant and small (~ 0.3). k is the rate constant for sulfur removal from the slag by the slag-gas reactions. It is expected to be dependent on (i) slag chemistry, (ii) foam volume/void fraction/slag-gas interfacial area, (iii) gas composition (% H_2 and % H_2O) and flowrate, (iv) type of coal/coke, i.e. H_2 and H_2O content in coal, and (v) blowing practice and other operating parameters.

The relationship between α and k obtained from steady-state conditions may be utilized in either the differential equation or the integrated equation to calculate the sulfur content as a function of time during non-steady situations. Data collected during the horizontal vessel campaign were analyzed, and this analysis indicated that about 30% of the sulfur contained in the coal enters the slag and metal. The results were applied to predict the change in the sulfur content of the slag and metal with time in experiments where batch additions of FeS_2 were made to the slag. Figure 7 shows the change in the sulfur content of the slag and metal with time. At t = 0, 223 kg of FeS_2 was added to the slag. The solid line shows the predicted sulfur content in the slag, while the dashed line indicates the predicted sulfur in the metal. As is evident, there is good agreement between the predicted and measured values.

HYLSA GAS PHASE TEST RESULTS

H_2S Removal in Reduction Shaft

Data from the direct ironmaking smelter operation at the Universal pilot plant showed that about 80 percent of the sulfur input appeared in the smelter offgas. Because this gas ultimately is used in a reduction shaft to produce wustite for the smelter, trials were conducted at HYLSA to determine if sulfur in the gas phase could be effectively removed in the reduction shaft.

These trials were conducted with the simulated smelter gas composition (postcombustion of about 40%) and temperature (900 C) shown in Table III. H_2S (the expected primary sulfur species in the smelter gas at 900 C) in the gas was produced by injecting carbon disulfide. Because of limitations in the injection system, the H_2S in the gas phase was limited to about 1100 ppm. The first test was conducted with only pellets charged to the shaft to produce wustite. In this test, about 63 percent of the input sulfur appeared as FeS (0.07% S) in the wustite (see Table III). The H_2S in the shaft offgas from this test was 395 ppm (37% of S in).

In the second test (see Table III), calcined dolomite (about 85 kg/t Fe) was added to the shaft. During this test, both wustite and dolomite captured sulfur. The sulfur content of the wustite and dolomite in the shaft product were 0.078 and 1.34 percent, respectively. The sulfur was distributed as follows: about

FIGURE 7

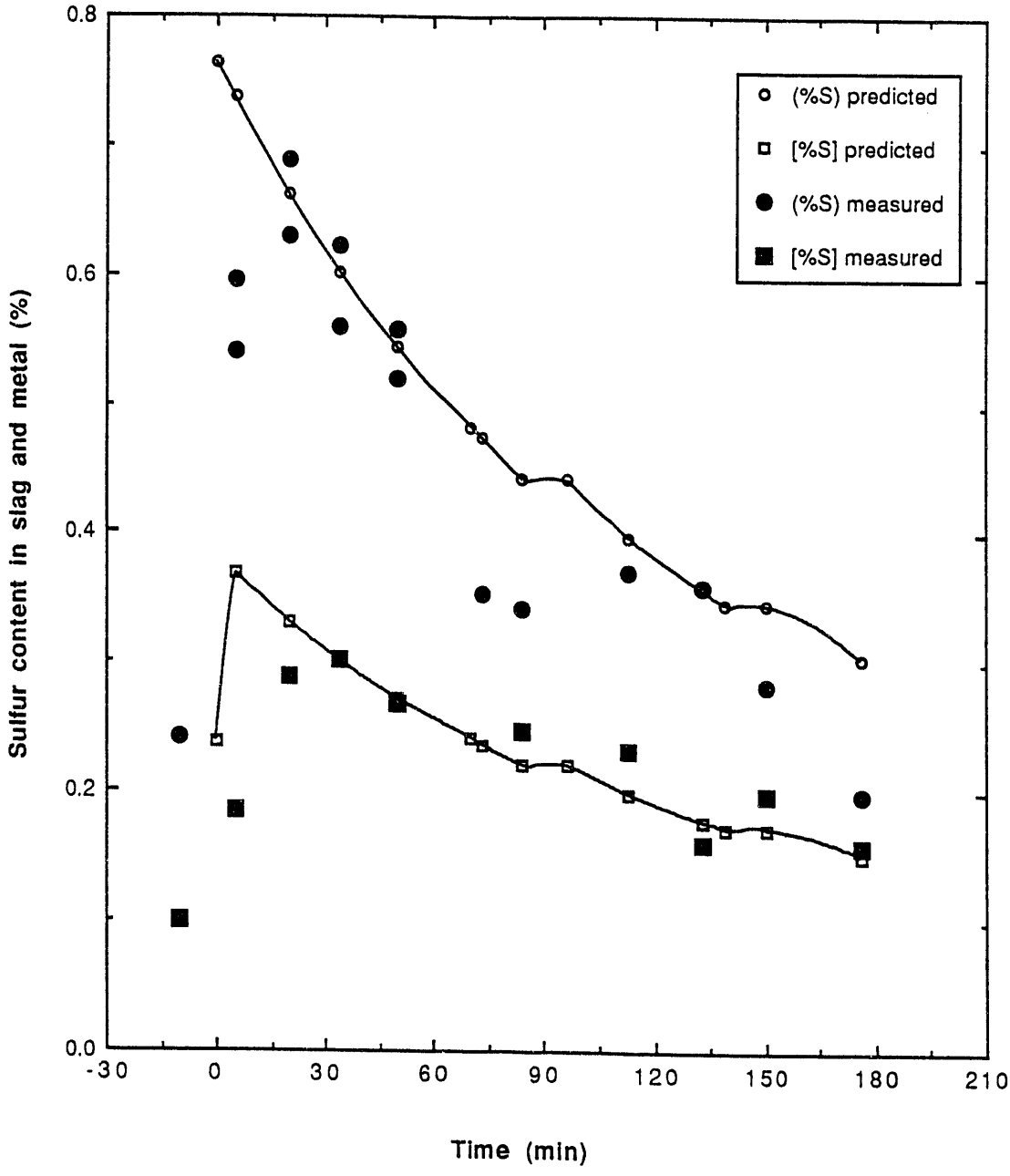

Comparison between predicted and measured sulfur contents during batch addition experiment in Trial H-19. Predicted values assume constant sulfur partition ratio.

52 percent in the wustite as FeS, about 39 percent in the dolomite as CaS, and about 9 percent in the shaft offgas as H_2S. The H_2S in the offgas was 120 ppm.

The above results are consistent with equilibrium calculations. For example, the phase diagram shown in Figure 8 for the Fe-Ca-S-O system 900 C shows that both FeS and CaS could form and were formed during the trials. Furthermore, the analyses of the sulfur in the wustite and in the gas during these trials were reasonably consistent with those predicted from equilibrium calculations.

Further studies of the pellet microstructure showed that pyrrhotite, a bronze-colored form of FeS, forms primarily on the surface of the pellet. No sulfur was observed in the pellet core.

These trials have been helpful in understanding how the shaft process can remove sulfur from the gas phase.

TABLE III

Sulfur Removal Test Information

Gas Composition to Shaft

CO	40.2 %	39.5 % PC
CO_2	27.2 %	
H_2	17.1 %	
H_2O	10.2 %	
H_2S	~1100 ppm	
N_2	Balance	

Test Results with Only Pellets Charged to Shaft

Sulfur in Pellets as FeS	63 % (0.07 % S)
Sulfur in Offgas	37 % (395 ppm H_2S)

Test Results with Pellets and 85 Kg Calcined Dolomite/t Fe Charged to Shaft

Sulfur in Pellets as FeS	52 % (0.078 %)
Sulfur in Calcined Dolomite	39 % (1.34 % S)
Sulfur in Off-Gas	9 % (120 ppm H_2S)

Proposed Integrated Process Flowsheet for Sulfur Management

A sulfur balance model has been developed which permits one to investigate the effects of alternative process flowsheets and operating strategies. The model incorporates an H_2S scrubber system for removing H_2S from the gas in the gas conditioning loop for the shaft. Investigations show that the H_2S scrubber system can also process the shaft offgas to decrease its H_2S content to 40 ppm or less.

FIGURE 8

ISOTHERMIC SECTION OF THE Fe-Ca-S-O

SYSTEM AT 900 C

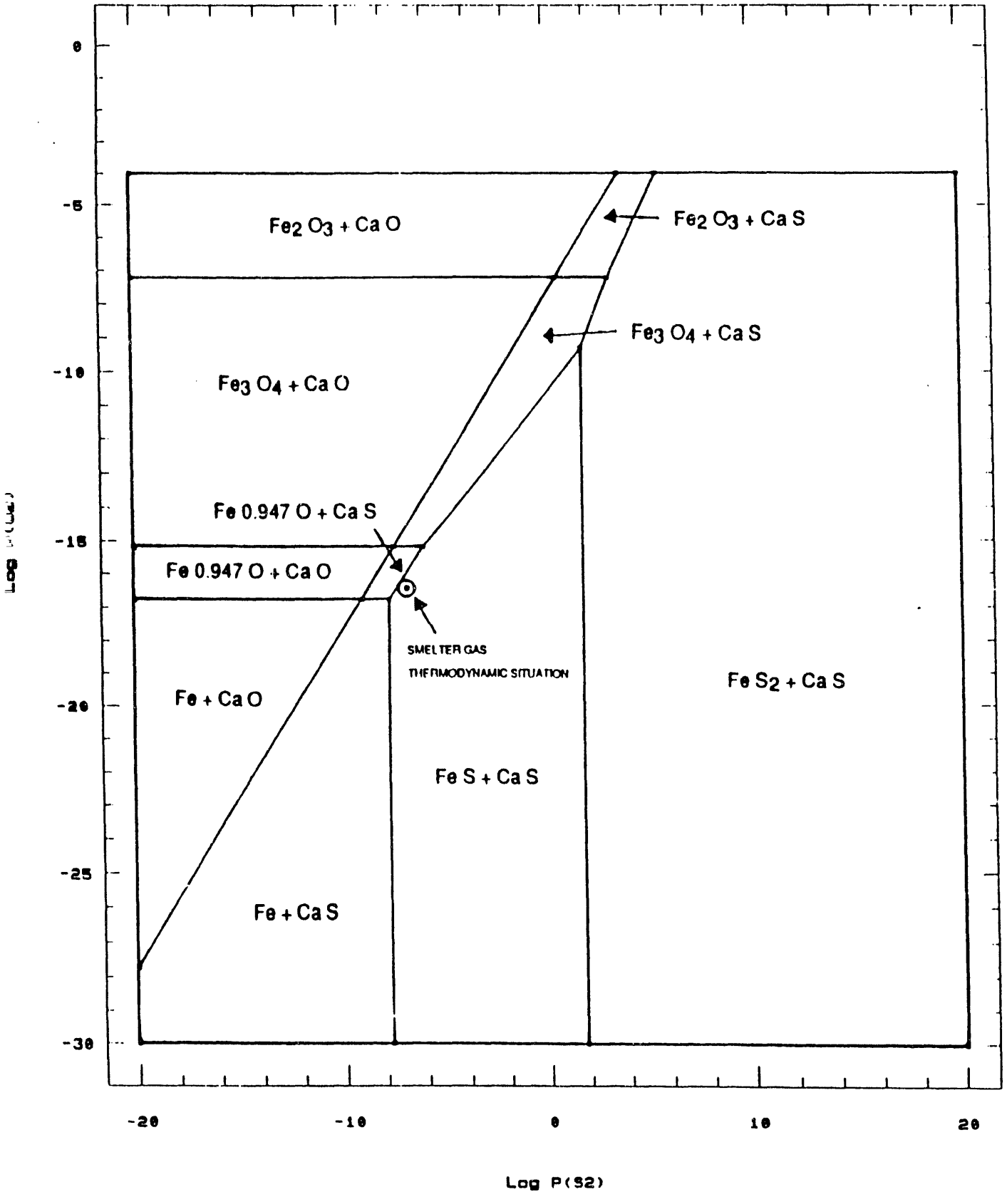

Thus, the H_2S scrubber system can make the process environmentally acceptable from a sulfur discharge point of view.

This model has been quite useful in evaluating various strategies and will be incorporated into an overall process model.

PRINCIPAL PROCESS SENSORS

Gas and Dust Analysis

Good continuous gas analysis has been successfully obtained from the offgas duct at the pilot plant. Much time and effort has been taken to properly prepare the gas sample for the mass spectrometers. The offgas analysis is not available for one minute in every 15 minutes while the system is being purged with nitrogen to clean the filter system.

Work has continued with measuring and sampling the dust. The primary dust measurement comes from the filtering of quencher water samples. The dust loading data generated from the quencher samples matches quite closely the amount of sludge removed from the clarifier. In-line samples of the dust have been taken for dust loading and chemical composition, and the results are currently being reviewed. The installation of the third vessel and gas loop will enable better study of dust loading, dust composition, and the effects of dust recycling.

Temperature of Metal, Slag, and Gas

The temperature of the metal and slag are measured on line with the sensor lance. The sensor lance takes a metal temperature and sample and then retract about 1 meter to obtain a slag temperature. The metal and slag temperatures are also taken during casting, and the metal temperature is taken during turndowns.

Measuring the temperature of the smelter offgas has always been difficult, even with the use of expensive shielded high-temperature thermocouples. The sensor currently under evaluation is a high temperature, dual band, infrared ratio thermometer (Figure 9).

Continuous and/or Intermittent Sampling of the Slag and Metal

Slag and metal sampling is done on an intermittent basis. The metal and/or slag samples are obtained at least every 30 minutes. The sensor lance is used to collect most of the samples, although manual samples are taken at every turndown and when casting. The sensor lance slag samples are taken with a 1" pipe with holes drilled in it. This provides a good in-process slag sample that has not been reacted with oxygen or additional carbon when the sample is retracted. Some pipe samples are also saved and split open to determine the size fraction of the metal droplets and char particles.

FIGURE 9

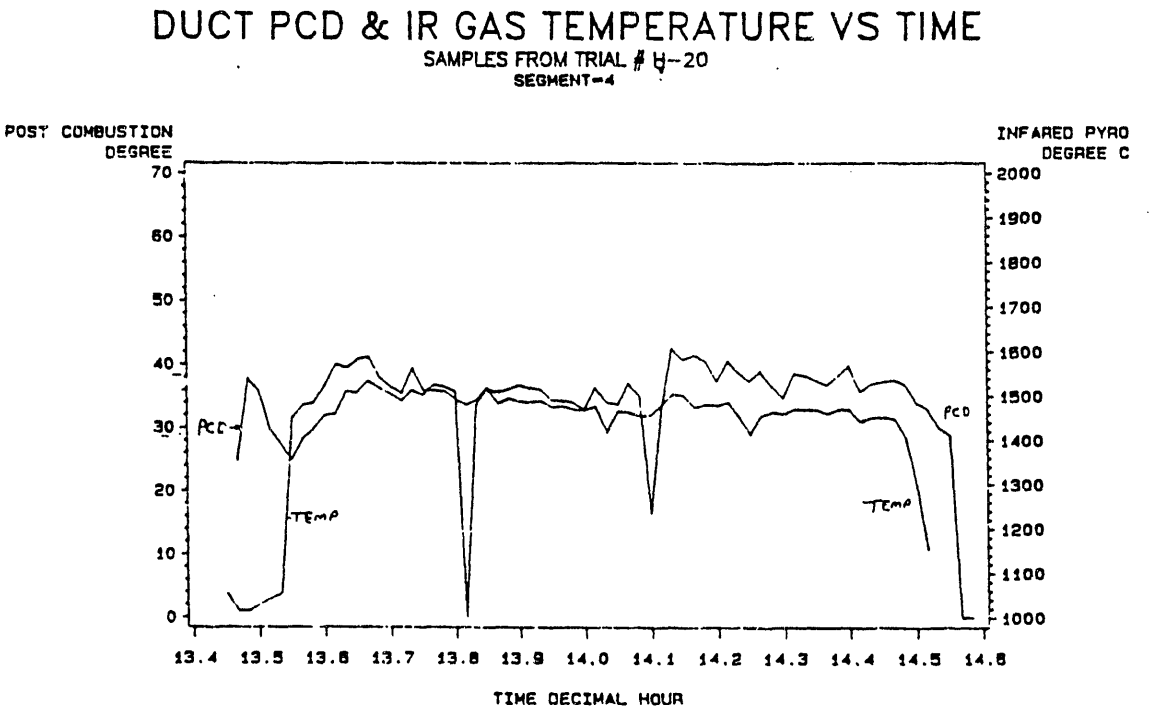

DUCT GAS POSTCOMBUSTION = (–)
IR PYROMETER = (–)

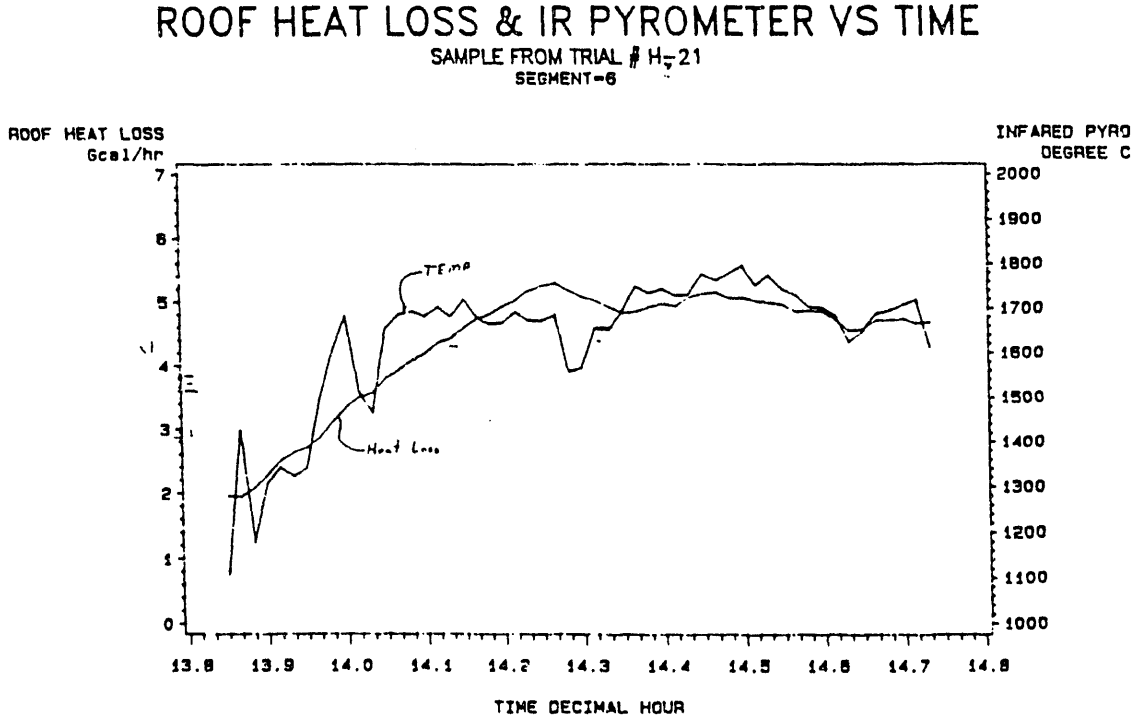

ROOF HEAT LOAD = (–)
IR PYROMETER = (–)

FIGURE 10

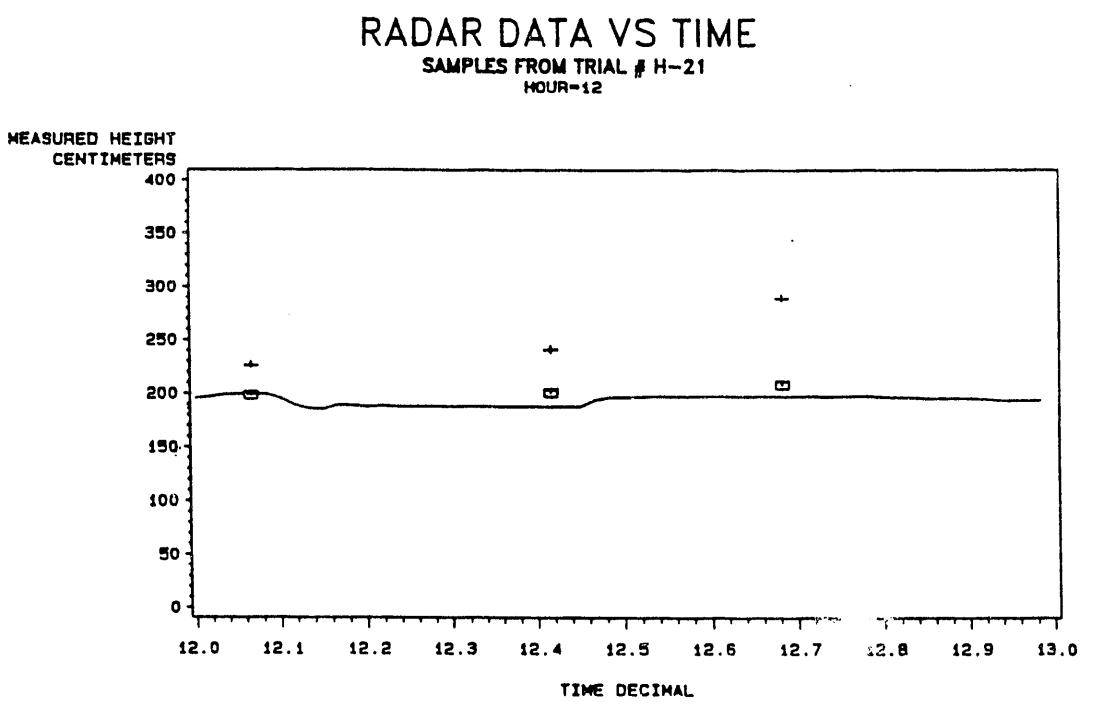

RADAR MEASURED FOAM HEIGHT = (-)
CHAIN SLAG MEASUREMENT = (SQUARE)
CHAIN SPLASH MEASUREMENT = (+)

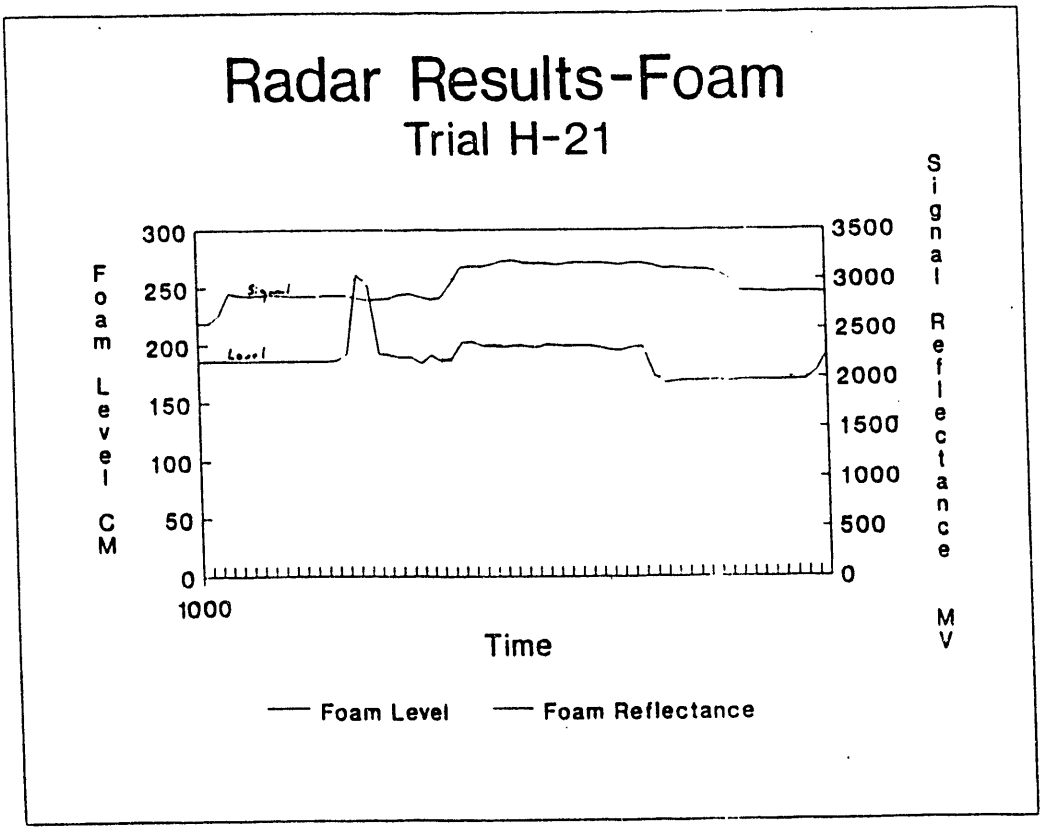

On Line Foam Height Detection

On an intermittent basis, a chain is attached to the sensor lance to obtain slag heights. The chain is attached before a normal sensor lance temperature or sample is taken. The height of the slag on the chain is then measured and converted to a foam height based on the depth of the sensor lance into the bath.

A microwave radar device has been used to measure the slag height on-line. It appears that the slag reflects enough of the radar signal to allow this type of device to be used. However, it has been difficult to quantify the true origin of the reflections from the foaming slag. Work is continuing on correlation of information received from the radar device and the sensor lance readings. To date it appears that the radar device could be a useful tool in determining the slag level in the vessel.

The radar transmitter/receiver and antenna are housed in a 12" pipe that extends through the roof of the vessel to the hot face. The assembly is kept cool with a nitrogen purge through the antenna. The transmitter is isolated with a teflon plug above the purge point. The signals from the receiver are then sent to the control room where they are processed. The position of the transmitter-antenna was near the center of the vessel (Figure 11). It could not placed on the center line because of interferences. This caused some problems because a false signal could be received from the vessel sidewalls. Also, when the bottom of the radar port would become partially obscured with slag buildup, the signal was partially obscured. The radar device would work very well for a time and then not respond well. More work will be necessary to improve the reliability of the information received from the device and its interpretation.

Quartz Window

In an effort to look inside the process, quartz windows were installed in the man door of the vessel. A 4" window was installed in the man door, and a 6" window was installed in a refractory sleeve just inside the hot face. A video camera was installed outside the door for viewing the window, and the picture was displayed and recorded in the control room. The location of the hot face window was critical. If it was too far back, the slag and metal droplets would freeze on the window. If it was too close, there were problems holding the window in place. After several attempts, good pictures of the top of the foaming slag were obtained.

Refractory Heat Losses and Wear

A series of triple thermocouples inserted in several locations was used to monitor the heat losses through the lining. At each thermocouple location, the temperatures at the mid-point of the working lining, the interface between the working lining and the safety lining, and at the vessel wall were measured. When the first thermocouple failed, it provided an indication of the vessel wear. To measure the heat losses through the water-cooled portions of the

FIGURE 11

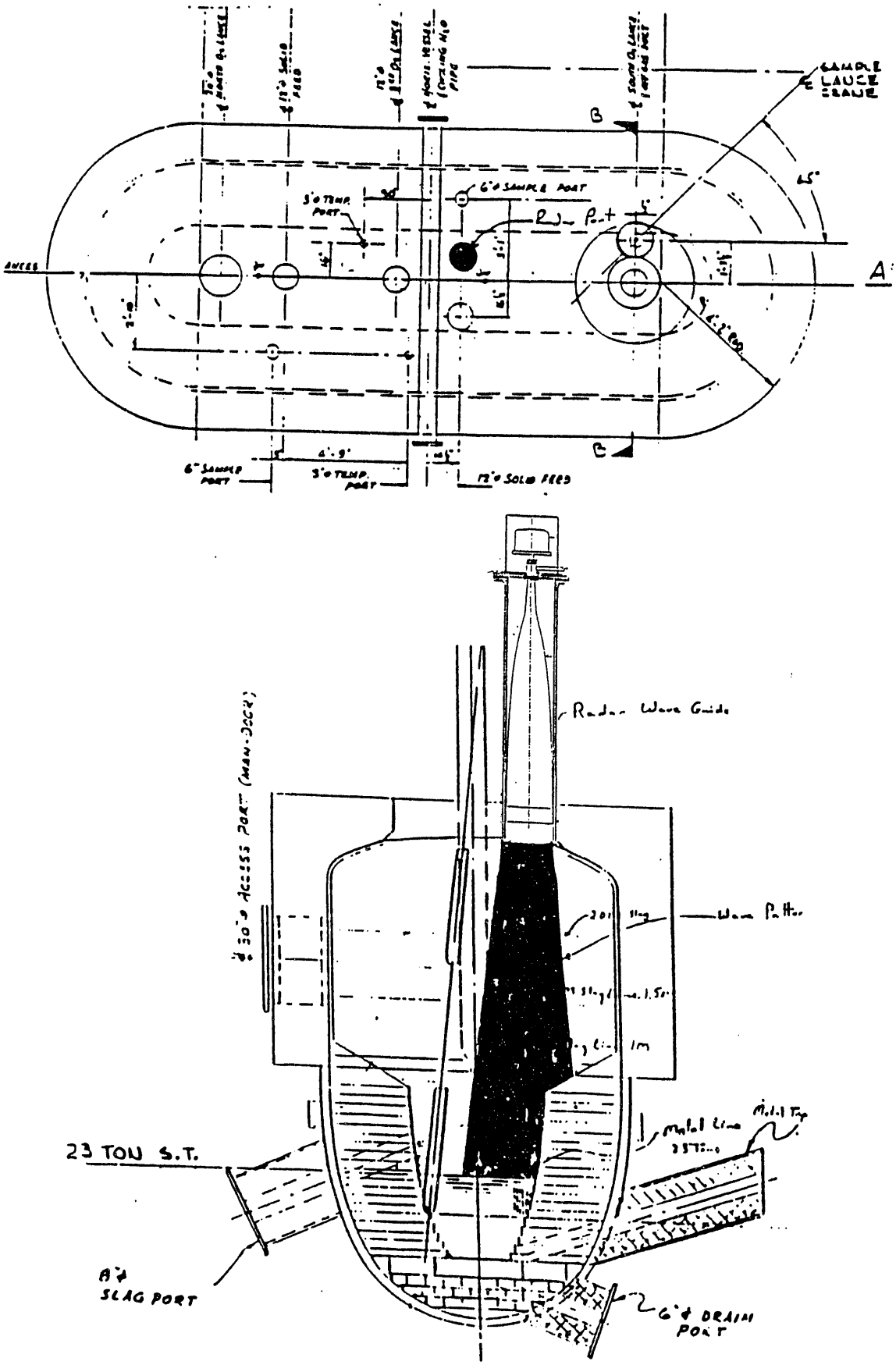

LOCATION OF RADAR DEVICE

vessel, the flow of the cooling water and the in and out temperatures were measured. After every trial the refractory lining was measured to determine the wear for that trial.

Four lining campaigns were conducted with the horizontal vessel. Figure 12 shows wear patterns for the horizontal vessel that are quite similar to those for the vertical vessel.

The wear rates observed in the horizontal smelter were undoubtedly influenced by the periodic nature of the operations. Some oxidation and accelerated wear were obvious on the initial preheat on magnesia-graphite refractories. The extent of oxidation on subsequent preheats on a given lining are not known but undoubtedly were reduced by the presence of a slag coating. On any commercial smelter, this effect would obviously be minimized. (Refractory samples from used brick at the end of a given campaign did not show any obvious hot face carbon loss.)

Thermal spalling or cracking effects from the periodic operation were also not obvious on the magnesia-graphite refractories but were apparent as spalling on the original burned-impregnated brick.

Used sample examination on the magnesia-graphite brick indicated that the main wear mechanism was related to high-temperature erosion-corrosion. This type of mechanism is known to be very temperature-related as wear increased by several orders of magnitude between 1600 and 1800°C. The most wear appears to have occurred in the postcombustion areas where temperatures were at maximum. Control of consistent process temperatures in this zone will be the most important factor in smelter refractory life.

FIGURE 12

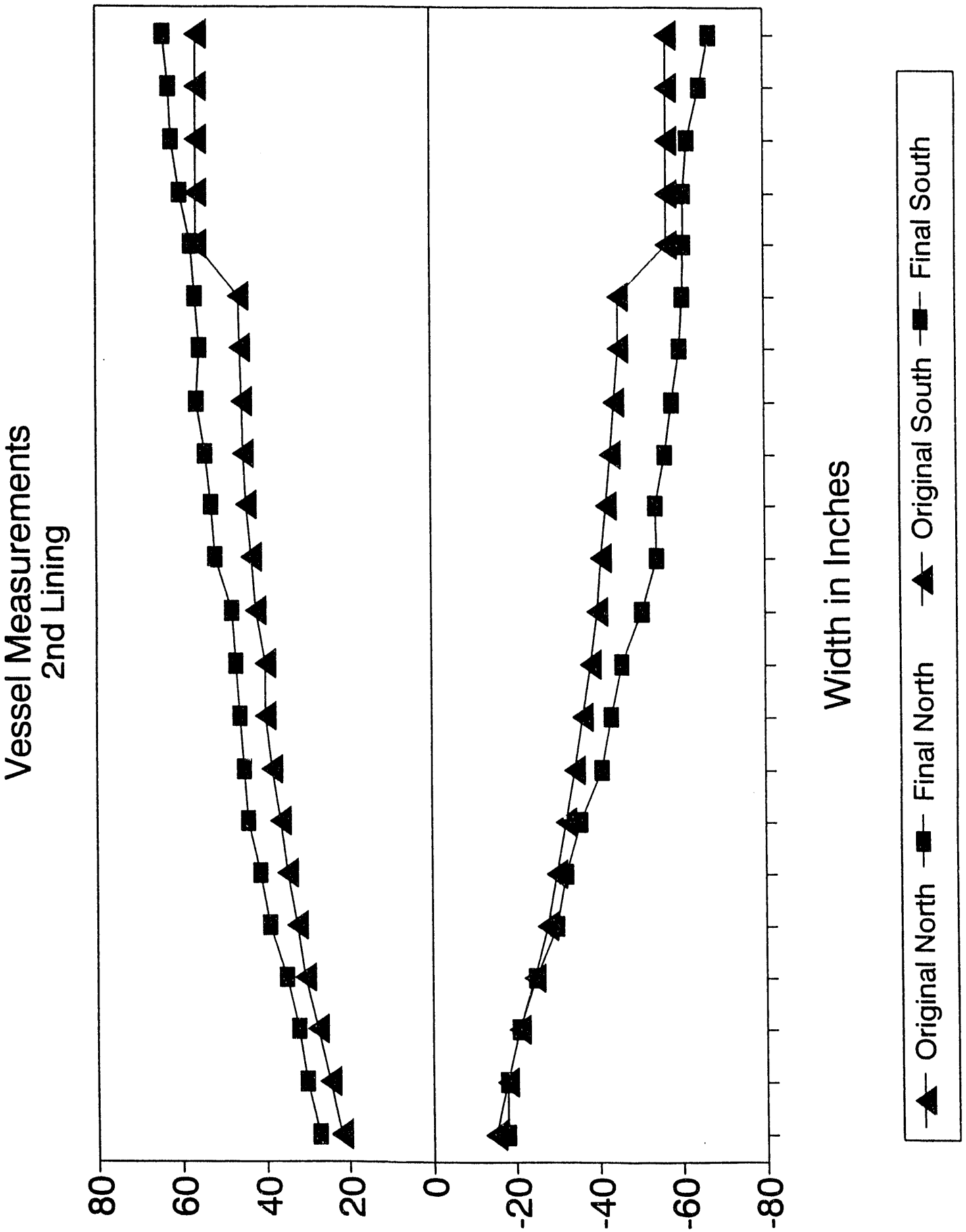
Vessel Measurements
2nd Lining
Width in Inches
80
60
40
20
0
-20
-40
-60
-80
Original North
Final North
Original South
Final South

TASK 10 - DESIGN OF GAS CLEANING AND TEMPERING LOOP

In late 1991 the decision was taken that the gas cleaning and tempering facility would be designed, constructed, and tested in conjunction with the third smelter. It was also decided at that time that, while offtakes would be provided to connect this facility to a prereducer, the prereducer would not be built in the current phase.

Pre-engineering meetings began early in January, 1992, with the selected EPCM contractor (Hatch Associates). The scope and flowsheets were approved by the end of February and the final layout shortly afterwards.

Equipment specifications were prepared and put out for bid, and by late summer all major components were on order.

As the construction engineering was completed, contract specifications were prepared for the civil, mechanical, piping, electrical and instrumentation, and process control work. By the end of October, 1992, all of these contracts had been put out for bid; in November the final contractors were selected and contracts let.

The horizontal smelter program (Task 9) concluded as planned in September, and work began immediately at the site, demolishing and removing gas cleaning and other adjacent equipment that would not be needed for Task 10.

The civil contractor was on site before the end of October, and all foundation and site work was completed by mid-November.

The mechanical/structural/piping contractor is now working on site, and major components are arriving weekly. The electrical contractor is currently mobilizing.

The project is on schedule.

Figure 13 is a schematic of the offgas system.

FIGURE 13

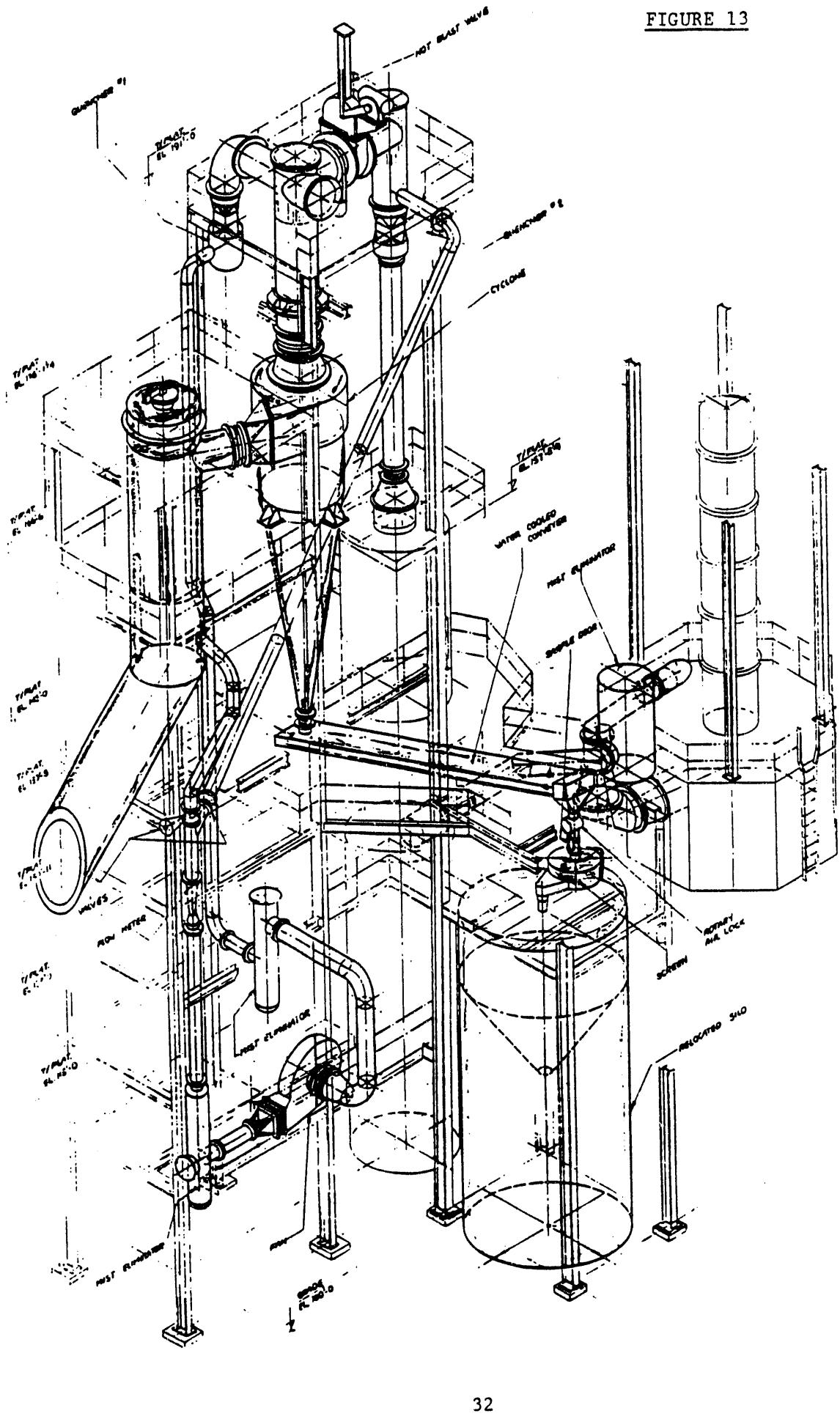
HOT BLAST VALVE
CYCLONE
WATER COOLED CONVEYER
HEAT ELIMINATOR
SAMPLE DOOR
VALVES
FLOW METER
ROTARY AIR LOCK
SCREW
RELOCATED SILO
AMERICAN IRON & STEEL INSTITUTE
DIRECT STEELMAKING PILOT PLANT
O.& B TEMPERING LOOP
ISOMETRIC GENERAL ARRANGEMENT
10102
M-010
P3
HATCH ASSOCIATES

TASK 11 - DESIGN, CONSTRUCTION, AND OPERATING PLAN FOR THE THIRD, PRESSURIZED SMELTER

Mannesmann Demag Corporation was contracted in January, 1992, to do a preliminary study on the design of the third smelter facility. This initial study was approved, and in May, 1992, Mannesmann Demag was given a further contract to design, detail, and supply the major components for this pressurized smelter and associated equipment.

In June, 1992, with DOE approval, Hatch Associates was awarded a contract to do the construction engineering and construction management of the project.

Coordination meetings between AISI, Hatch, and Mannesmann Demag were begun in late July and have continued on a regular basis since then because of the importance of the third vessel to the project and the tight schedule for its installation.

Site clearance commenced shortly after the shutdown of the horizontal smelter in September, and all major components no longer required were removed and the site cleared by mid-October.

As design drawings were completed, specifications were prepared and sent out for bid. By the end of October, all major equipment, including the redesigned cone and cooling systems, were on order. Some deliveries have already occurred.

Specifications for all the construction contracts were prepared by Hatch as the drawings were completed.

A contract for the civil work was let in early November, and foundations are underway. A contractor has also been chosen for the mechanical and piping/structural work and is currently mobilizing. The remaining contractors will be selected shortly.

This project is scheduled for completion and commissioning in April, 1993.

Figure 14 is a schematic of the pressurized vessel.

Operating Plan

- A requirement for more long-term trials. Several five-day runs to demonstrate plant reliability will be conducted.

- Develop stable operating conditions to define clearly the main operating parameters (coal rate, yields, etc.). Longer-term operations to confirm the shorter-term results are required as part of the process variable confirmations.

FIGURE 14

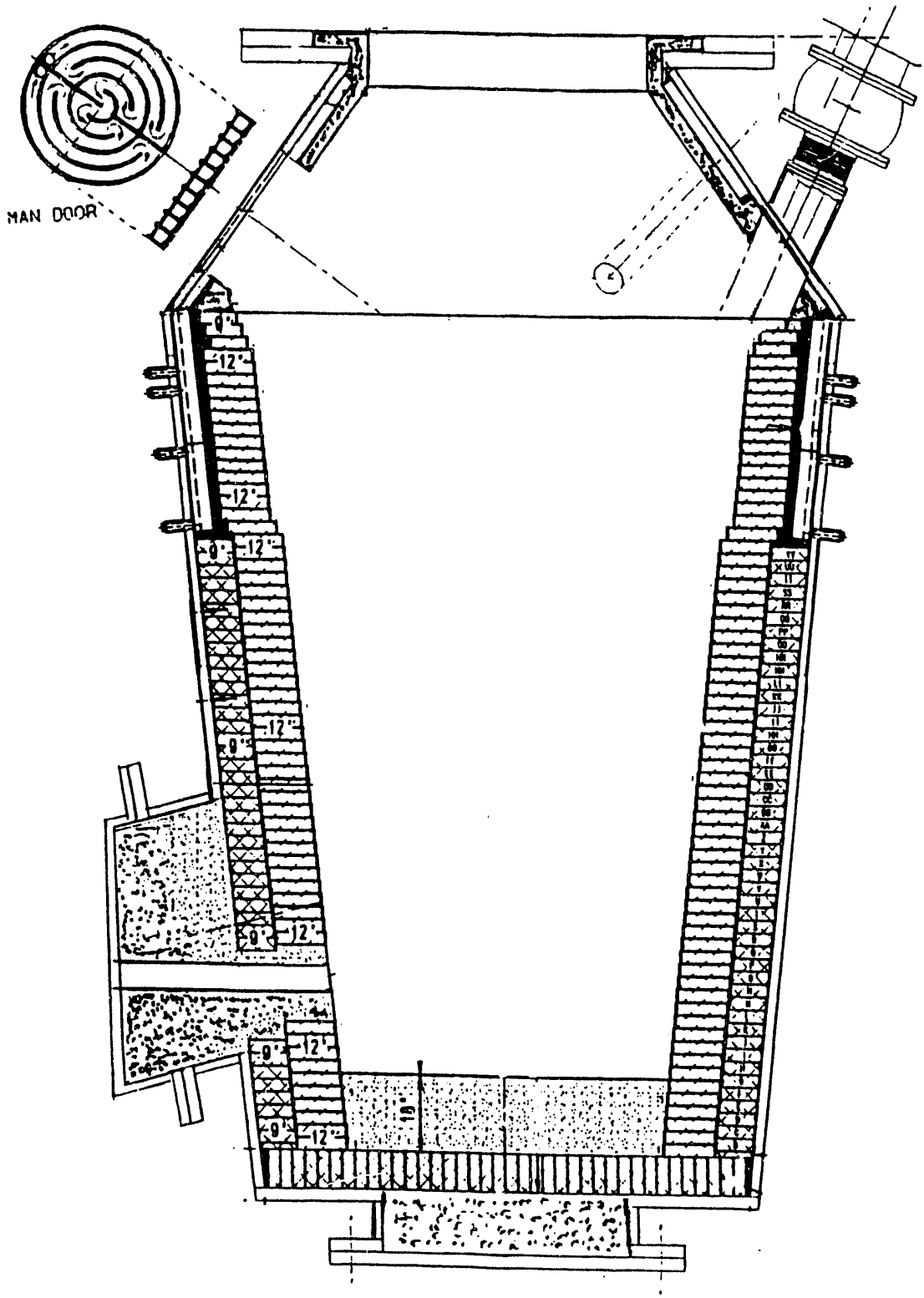

- Establish environmental discharges. Final permits for a demonstration plant would require determination of all discharge quantities in air, water, and solids for steady-state operation with the demonstration plant raw materials used in the pilot plant.

- Verify engineering parameters and equipment design for scale-up.

- Coal/carbon injection into slag.

- Determine heat transfer to the bath during long-term operation to confirm or improve the process operation.

- Refine operating process control models and model parameters for long-term and safe operation of the demonstration plant. Requirements for the process models are much more onerous than for the pilot plant because of the quantities of material, production rates, and level of experience of the operators. Optimization of these areas is required in the time leading up to the development plant.

- Test alternate coals (what is maximum sulfur level that can be handled). Tests of demonstration plant coals, higher sulfur coals, and/or other cheaper coals to define improved plant economics are desirable, as are tests on recycle sulfur and alkali loads in the gas tempering loop.

TASK 12 - 350,000 TON/YEAR DIRECT IRONMAKING DEMONSTRATION PLANT

1. Current Status of Preliminary Engineering

   a. The Mannesmann Demag Basic Study for a commercial direct ironmaking plant was completed and submitted to AISI in early November, 1991.
   b. This study confirmed "considerable potential for technoeconomic advantages of the AISI direct ironmaking process" and recommended proceeding with a feasibility study for a high-capacity demonstration plant.
   c. In May, 1992, the Project Board approved a Mannesmann Demag proposal for a study for a direct ironmaking plant of 350,000 ton/year. This study was delivered to AISI in December, 1992. It included layouts, facility requirements, and projected capital costs.

2. Major Components of the Facility

   a. There are four major components of the facility:

      (1) The smelter building which would contain the smelter and the bin and hoppers of the materials feed systems, as well as the cast house. The vessel tapping will be a conventional blast furnace casting arrangement. There will also be maintenance areas for lances and areas for spare parts and refractory storage.
      (2) The gas cleaning and tempering system, consisting of cyclones, dust injection system, scrubbers, gas desulfurization system, and the gas cooling recycle loop.
      (3) The prereducing moving bed shaft of the HYL type which produces wustite from the hematite pellet feed stock, along with its associated day bins, and pneumatic transport system to transport the preheated wustite to the vessel.
      (4) The oxygen producing plant of some 900 tons per day capacity to supply the required gases for the operation of the plant. Peripheral requirements include a substation to provide required electric power, all necessary fluid utilities, a water treatment plant, ore and coal storage and screening facilities.

   b. The smelter itself is a refractory-lined vessel with water-cooled panels in the upper barrel and cone sections to help control the refractory wear in the upper portion of the vessel without incurring a severe penalty for heat losses.

TASK 13 - LABORATORY RESEARCH PROGRAMS

Carnegie Mellon University

Reduction Process Model

The fundamental kinetics of the reduction reactions (9) and (10) have been studied.

(9)

$$(FeO) + C\ (char) = Fe + CO$$

(10)

$$(FeO) + \underline{C}\ (Fe) = Fe + CO$$

Typical results for reaction (9) for spheres are shown in Figure 15. In the smelting process the overall rate of reduction (R) is the sum of the slag-metal (R_{SM}), slag-metal drop ($R_{S\text{-}D}$) and slag-char ($R_{S\text{-}C}$).

(11)

$$R = R_{SM} + R_{SD} + R_{SC}$$

The rates can be calculated from the rate constants determined in the laboratory experiments and the surface areas computed from pilot plant samples.

(12)

$$R = (k_{SM} A_{SM} + k_{SD} A_{SD} + k_{SC} A_{SC})\quad (\%FeO)$$

This model has been successful in predicting the rate of reduction and the factors which influence the rate.

Slag Foaming

Slag foaming is an important phenomena in bath smelting. It may limit the production rate, and more effective postcombustion and heat transfer can be obtained using the foamed slag.

Dimensional analysis: Recent work indicated that the foam index is a function of bubble size, i.e. inversely proportional. A

FIGURE 15

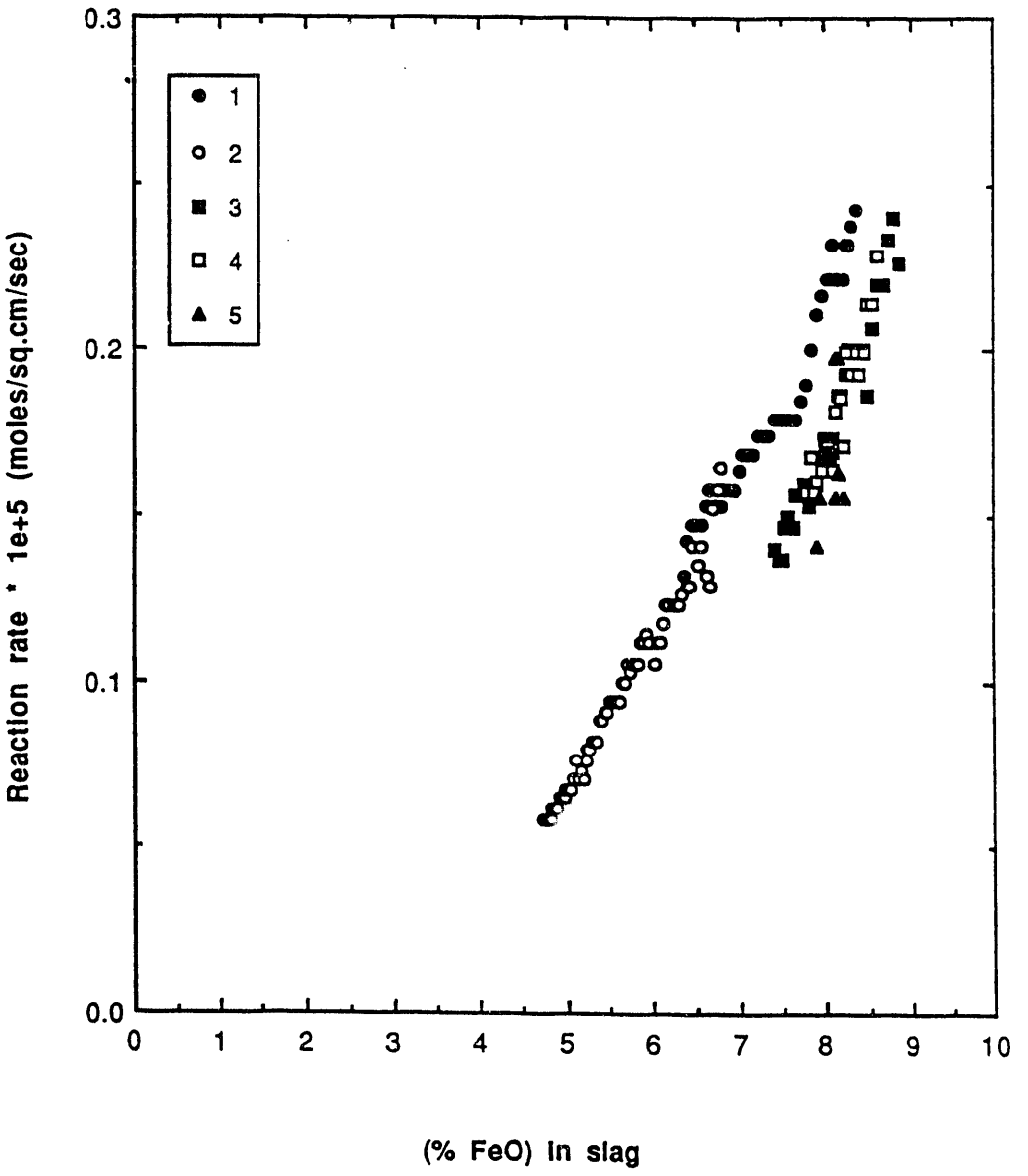

Reaction rate vs FeO content of slag for reduction by carbon spheres.

1. Coke sphere : Diameter = 1.5 cm : 2. Coke sphere : Diameter = 1.42 cm.
3. Graphite sphere : Diameter = 1.33 cm : 4. Graphite sphere : Diameter = 1.29 cm.
5. Coal char sphere : Diameter = 0.91 cm.

generalized dimensional analysis was performed from which the foam index could be predicted from the slag properties.

The following three dimensionless groups can be obtained based on the principle of dimensional homogeneity:

(13)

$$\pi_1 = \frac{\Sigma \mu g}{\sigma}$$

(14)

$$\pi_2 = \frac{\mu^4 g}{\sigma^3 \rho}$$

(15)

$$\pi_3 = \frac{\rho^2 D_b^3 g}{\mu^2}$$

where,

Σ: foam index, sec;
μ: slag viscosity, g/cm·sec
σ: slag surface tension, g/sec^2
ρ: slag density, g/cm^3
g: gravitational acceleration, cm/sec^2
D_b: average bubble diameter, cm

The dimensionless group π_1 is denoted as N_Σ. Further, π_2 and π_3 are recognized as Morton's number (Mo) and Archimedes number (Ar) respectively. The Morton's number signifies the ratio of the viscous force to the surface tension force, and the Archimedes number describes the ratio of the buoyancy force to the viscous force. Therefore, the following equation can be written:

(16)

$$N_\Sigma = C \cdot Mo^\alpha Ar^\beta$$

where α and β are exponential coefficients.

Hence, the dimensionless numbers N_Σ, Mo, and Ar were calculated from the measured foam index, average bubble diameter, and the slag physical properties. By taking the logarithm of both sides of equation (16) and carrying out a multiple component linear regression analysis, coefficients α and β and the constant C were obtained. The

final result of the dimensional analysis is described by the following equation:

(17)

$$N_\Sigma = 900 \cdot Mo^{0.39} Ar^{-0.28}$$

Considering experimental error, the coefficients can be approximately taken as 0.4 and -0.3. The gravitational acceleration is 980 cm/sec^2, so the foam index is given by:

(18)

$$\Sigma = 1.83 \frac{\mu^{1.2}}{\sigma^{0.2} \rho D_b^{0.9}}$$

Figure 16 shows the plot of $\ln(N_\Sigma)$ versus $\ln(Mo^{0.4}Ar^{0.3})$. The slope of the line that fits to the data points in this graph is unity. The excellent fit indicates the foam index can be predicted within $\pm$ 10%.

Effect of pressure on slag foaming: In this experiment, the argon gas was injected into the liquid slag (34% CaO, 37.5% SiO_2, 5% FeO, 14% Al_2O_3, and 9.5% BaO) by a single orifice alumina nozzle (I.D. = 1.75 mm) while the pressure was kept at about 1.9 atm. The foam heights at different gas flow rates were measured from the x-ray image. The result obtained was then compared with that measured at the normal atmospheric pressure (1 atm) with the same slag and at the same temperature.

As shown in Figure 17, the measured foam heights at the same volumetric gas flow rates or the same gas superficial velocities but at different pressures are equal. This means that the pressure does not affect the foam index. From the x-ray video image, no change in the bubble size is observed. The foam index is determined only by the slag physical properties when the bubble size is constant. Therefore, since the gas volume decreases with pressure, so will the foam height.

Effect of the type of injection gas: Preliminary experiments on the effect of the type of injection gas used to generate slag foaming were also carried out. In these experiments, helium gas was injected into a liquid slag (30%CaO-60%SiO_2-10%CaF_2) through an alumina nozzle (orifice I.D. = 1.75 mm) at 1500°C. The measured foam heights at different gas flow rates were then compared with those obtained with argon gas injection. The foam index of this slag at 1500°C was measured as 1.8 sec in previous experiments with argon injection. When helium gas was used to bubble through the liquid slag, less amounts of foam were generated compared to the case when argon was used. The foam index was reduced to 1.3 sec under the same

FIGURE 16

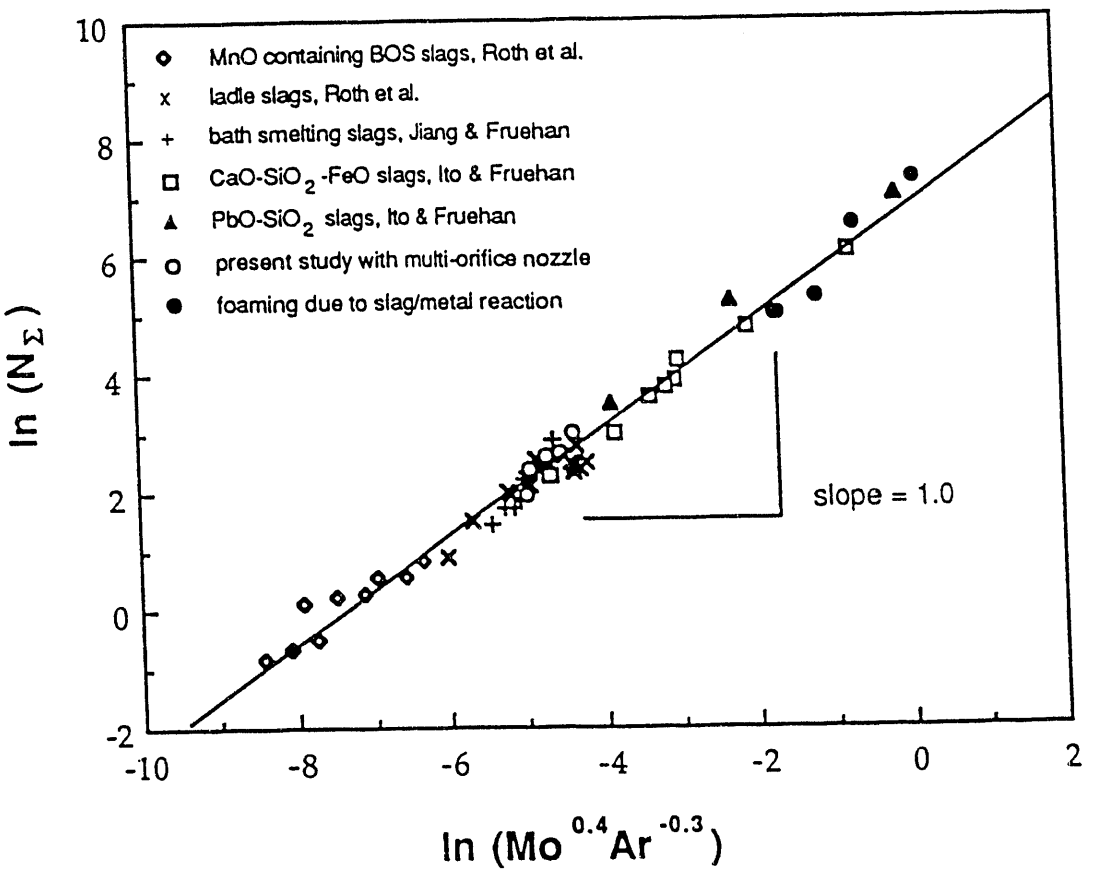

The result of the dimensional analysis considering the effect of the bubble size.

$$N_{\Sigma}=\frac{\Sigma\mu g}{\sigma}\ ;\quad Mo=\frac{\mu^4 g}{\sigma^3\rho}\ ;\ \text{and}\ \ Ar=\frac{\rho^2 D_b^3 g}{\mu^2}$$

FIGURE 17

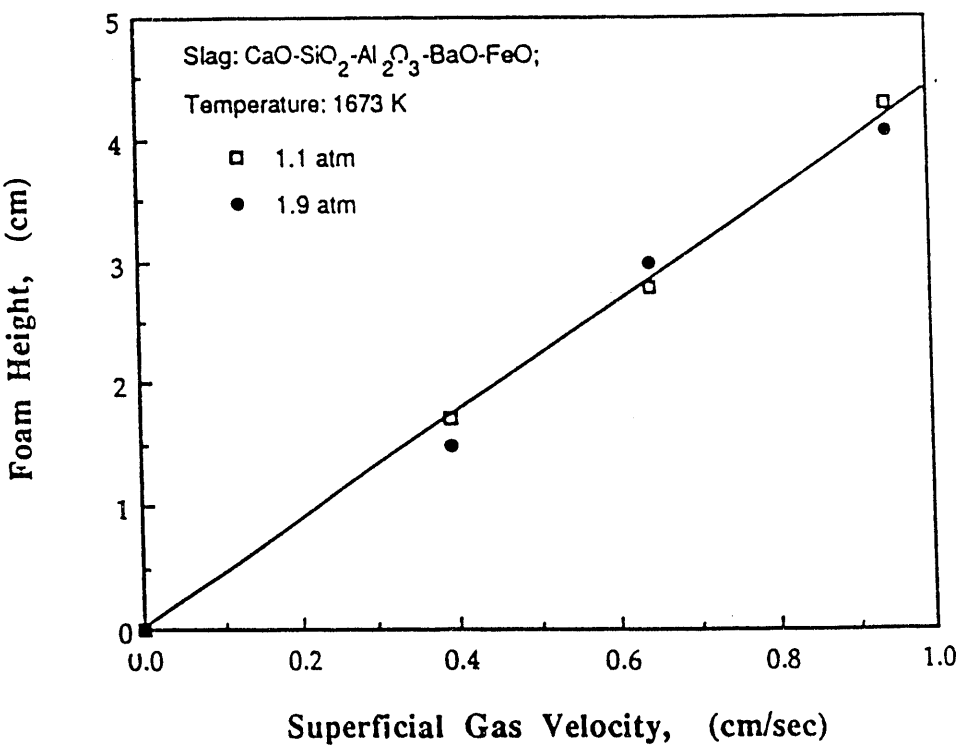

The effect of pressure on slag foaming.

experimental conditions. This may mean foaming from lighter gases (e.g., H_2) may result in lower foam heights.

Sulfur in Smelting

The behavior and removal of sulfur plays an important role in the overall process. CMU has conducted research on the rate of formation of H_2S from slag, rate of removal of H_2S by lime and dolomite, and desulfurization of smelter metal.

H_2S formation from slag: The rate of formation of H_2S by the ratio of H_2O with simulated smelting slag has been measured. The rate is relatively slow and appears to be controlled by transport of sulfur in the slag.

H_2S removal: It is possible to remove H_2S from the gas phase by use of CaO or dolomite CaO·MgO in the prereduction furnace or a separate reactor. The rate of sulfidation of CaO and CaO·MgO by simulated smelting offgases has been conducted as a function of particle size, temperature, and gas composition. Furthermore, the samples were examined after sulfidation in a SEM. The results indicate that the rate is controlled by diffusion of the H_2S through the product layer. It was found that the rate is proportional to H_2S pressure, decreases with increasing particle size, is not a strong function of temperature, and is faster for dolomite than CaO. From the results it is possible to predict the amount of dolomite required in the prereduction furnace and the final H_2S content of the gas. These results were used to guide the trials at HYLSA and were in agreement with their results.

Desulfurization of smelter metal: Extensive research was conducted to understand and optimize desulfurization of smelter hot metal. Smelter metal differs from the blast furnace metal in that there is no silicon present. The main focus of the work was to determine the amount of Si or Al required for rapid desulfurization. The results are summarized in Figure 18 where k is the first order rate constant. It was found that the addition of 0.1-0.2% Si would increase the rate by a factor of five. Al was less effective in increasing the rate. The rate was also determined as a function of temperature, particle size, and flux composition. A model for continuous desulfurization was developed. It was shown that a 10 tonne reactor could treat 50 tonnes/hour using about 10 kg of CaO-10%CaF_2 per tonne of metal. The metal could be desulfurized from 0.15% to 0.005% in such an operation.

Scale-up and Design Criteria

A simple model was developed to predict the theoretical production rate of a bath smelter considering both slag foaming and reduction. The volume available for foam is given by:

$$V_A = V_T - V_S - V_M - V_C$$

FIGURE 18

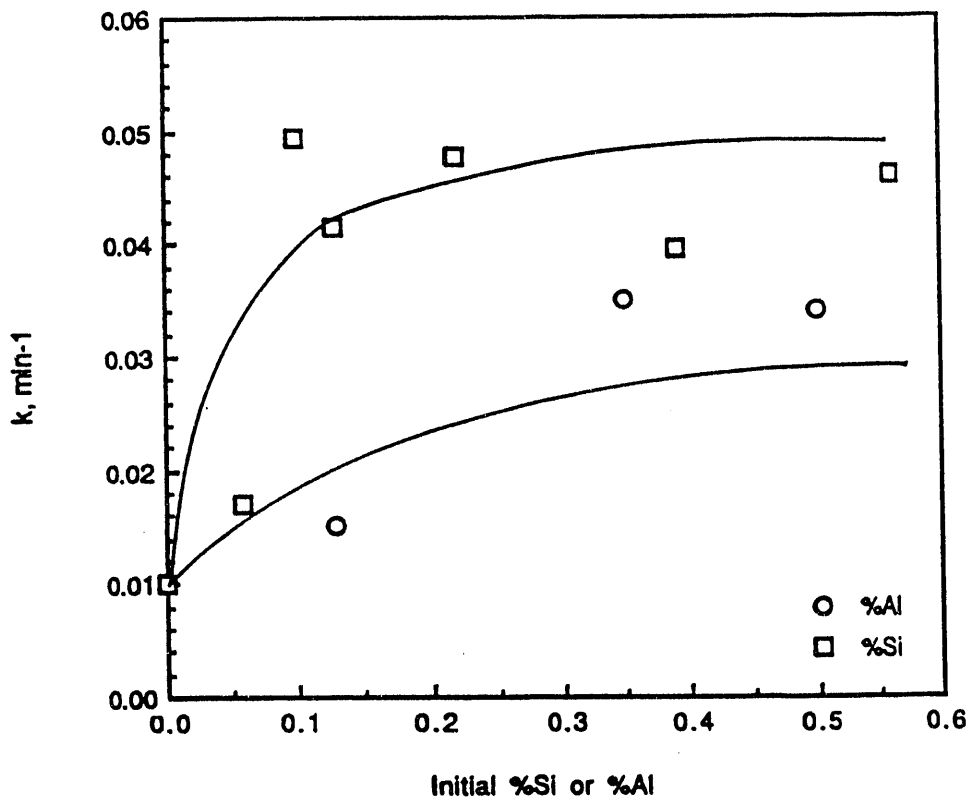

Rate constants for desulfurization using CaO-10%CaF_2 as a function of Al or Si content.

where V_A, V_T, V_S, V_M, and V_C are the available, total, static slag, metal, and char volumes. The rate of reduction or production is proportional to V_S. Therefore, as production increases, V_S must increase, decreasing the volume available for foam. Furthermore, as production increases, the gas generation and the foam volume increase.

These relationships are shown in Figure 19 for a generic 65 m^3 smelter in which the foam volume (V_f) and the available volume are plotted versus production rate. The intersection of the two curves gives the theoretical maximum production rate. As pressure is increased, the foam volume decreases and the maximum production rate increases. It is obvious that production rates of 10 tonnes/m^3 day, even considering the volume of the prereducer, are technically possible.

FIGURE 19

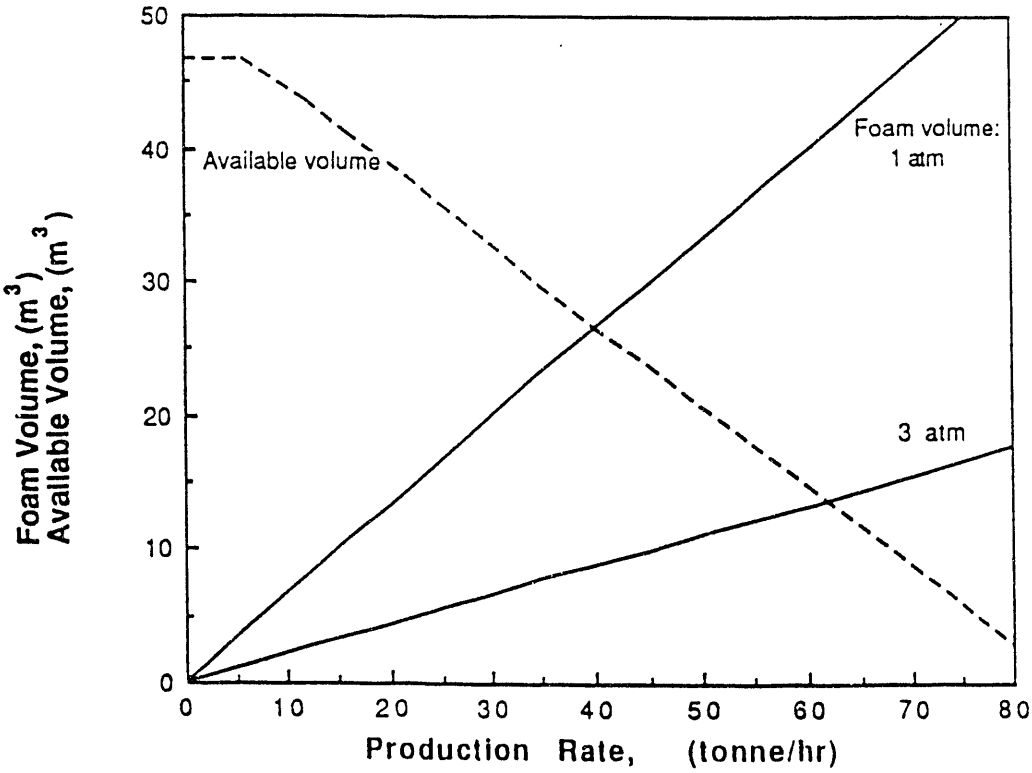

Foam volume and available volume for generic 100 m^3 vessel using 65 m^3 for smelting FeO.

McMaster University

Model for Oxygen Jet Combustion in Smelter

To improve our understanding of the oxygen jet trajectory and reaction rates, a mathematical model has been developed to describe the oxygen jet entrainment and postcombustion reactions. The model can be used directly for oxygen lance design and scale-up. The model results were compared with measurements in combustion chamber experiments conducted by Praxair (formerly Linde) for AISI.

The general shape of an oxygen jet delivered from the oxygen lance to the smelting vessel is shown in Figure 20. The jet entrains the ambient gas (fuel) and induces reactions within its domain. Along its trajectory, the jet spreads out with changes in temperature, composition, and direction. The jet behavior is mainly influenced by initial momentum and injection angle (lance design) and entrainment.

The mathematical model is based on Ricou and Spalding's jet entrainment model (J. Fluid Mechanics, Vol. 9, 1961) in which the mass entrainment rate is:

(19)

$$\dot{m} = k_e d_j u_j (\rho_j \rho_a)^{\frac{1}{2}}$$

where ρ_j and ρ_a are the jet and ambient gas densities, respectively, d_j is the jet diameter, u_j is the jet velocity, and k_e is an empirical entrainment coefficient. For low velocity and non-reacting jets, it was found that $k_e = 0.25$, as recommended by Ricou and Spalding, works very well. If the jet velocity approaches sonic velocity, or if there are reactions taking place in the jet, k_e has to be reduced to fit measured results.

The combustion rate in the jet is assumed to be controlled by the mixing rate of entrained fuel and jet oxygen, and is related to the entrainment rate, as proposed by Emmons and Ying (Proceedings of 11th {International} Symposium on Combustion, 1967):

(20)

$$R_{PC} = -k_r d_j u_j Y_{fu} \rho_j$$

where Y_{fu} is the fuel mass fraction in the jet and k_r is a reaction rate constant determined empirically.

By solving a set of one-dimensional ordinary differential equations for mass, momentum and energy conservation, the jet velocity,

FIGURE 20

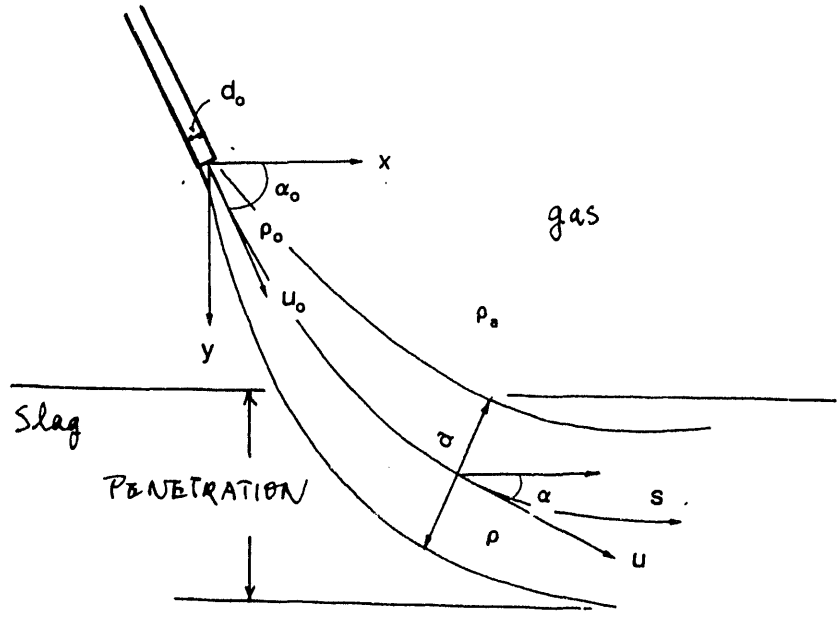

Schematic diagram of a jet trajectory

FIGURE 21

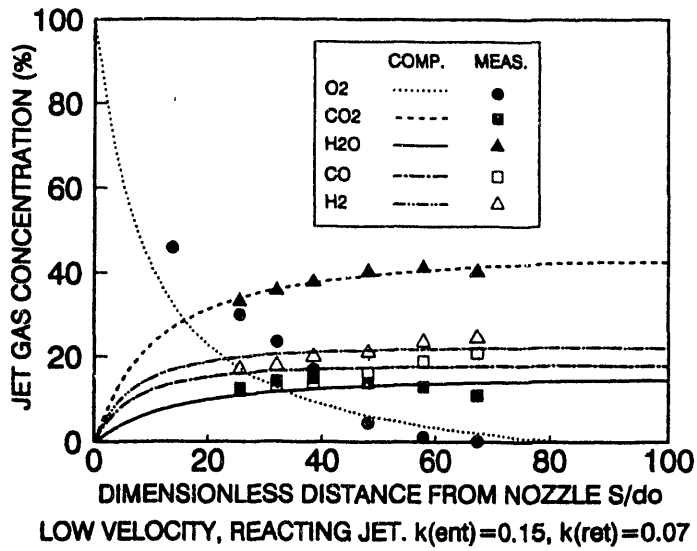

Comparison of jet gas compositions between model results and measurements (Praxair).

composition, temperature, size, and trajectory can be obtained. Figure 21 shows a comparison of measured and computed jet composition along its trajectory for a low velocity, reactive jet. The model is now available for detailed lance design for the smelting vessel.

Gas Jet Penetration Model

To describe the jet impingement on the liquid surface and penetration into the liquid, a separate model has been developed. This model predicts the intersection of the oxygen jet with the liquid slag surface and the maximum penetration depth of the jet into the slag. Basically, the jet penetration model is an extension of the jet combustion model described previously. When the oxygen jet with certain momentum and angle impinges on the liquid slag, it will penetrate into the slag, entrain the slag in the jet, and finally lose all its momentum and subsequently rise up. The maximum penetration depth depends on jet momentum and impinging angle, entrainment of liquid slag, and buoyancy force.

Data on jet (gas and gas/solid) penetration into various liquids available in the literature have been used to verify the model and to establish the value of the liquid entrainment coefficient. It was found that the liquid entrainment coefficient into a gas jet is substantially lower than gas-gas entrainment. Figure 22 shows a comparison between literature data on penetration depth and modeling results.

The oxygen jet combustion model and the gas jet penetration model were combined together to aid in the design of the oxygen jets in the AISI horizontal smelter. Figure 23 shows a calculated oxygen jet's distribution on the liquid slag surface at the gas/slag intersection for a particular operation condition. The oxygen concentration, jet temperature, and velocity upon impingement could also be determined. Nitrogen jet penetration depths and trajectories into slag from a horizontal tuyere for various modified Froude numbers, N_{Fr}', can be calculated from equation 21.

(21)

$$N'_{fr} = \frac{u_0^2 \rho_g}{g d_0 (\rho_l - \rho_g)}$$

This model will also be used for the design and scale-up of coal and iron ore injection systems.

FIGURE 22

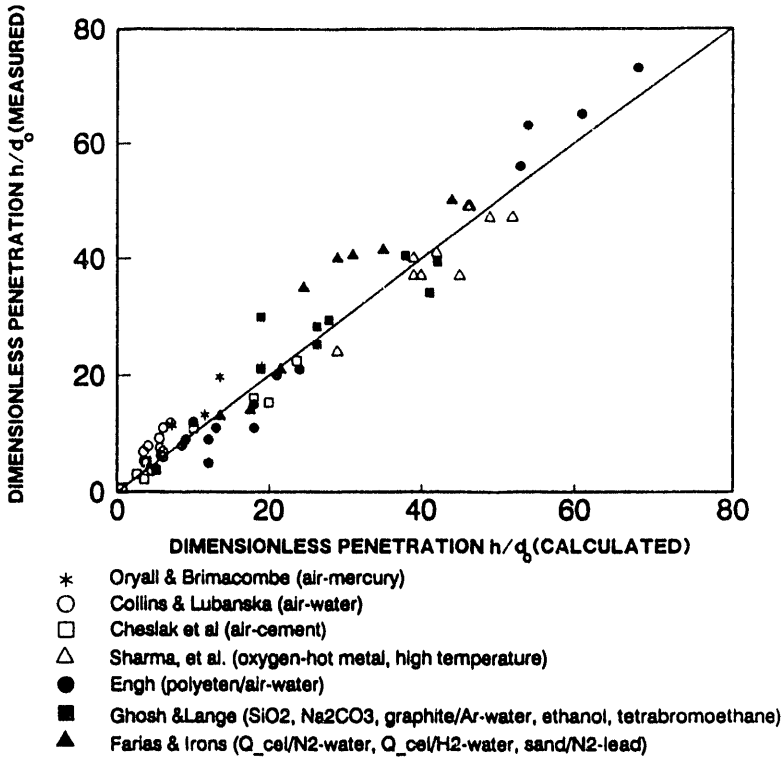

Comparison of jet penetration depth between model results and measurements (literature)

FIGURE 23

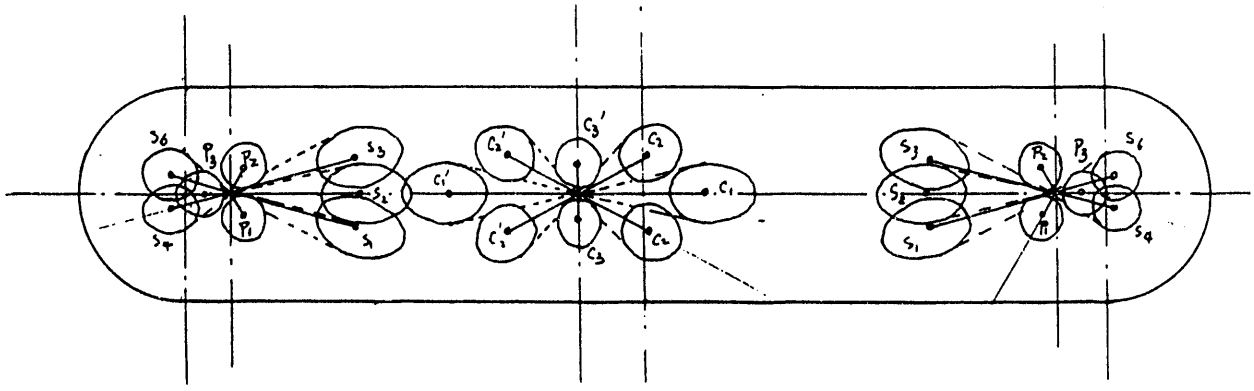

Calculated oxygen jets and foam slag intersection area PCD=40 %, Lance tip to slag surface distance=0.75 m

Praxair (Linde)

Extension of the Parametric Model to the Horizontal Smelter

A heat and material balance model for the two-zone smelter was formulated based on extending the one-zone parametric model developed for the vertical smelter. The model treated the horizontal smelter as two vertical smelters (two smelting zones) with material and heat flow between the zones. A hot metal back flow between smelting zones was incorporated into the model based on the experimental water model work by CMU and USS. Further refinement awaits input from the AISI Direct Steelmaking task force.

A detailed sensitivity analysis was performed to identify parameters which strongly influence the carbon balance calculation. The heat transfer in the headspace of the pilot plant pressurized smelter was estimated using the heat transfer model developed for the horizontal smelter (with appropriate geometry modifications). The analysis concluded that operating with a thin frozen slag layer in the water spray cone is not a viable option due to the excessive heat flux and thin steady- state lining thickness. A water spray design with a MgO lining and/or a mini-stave design with a MgO/graphite lining are preferred for the cone. A high alumina gunning mix is not recommended due to its relatively low thermal conductivity.

Visual Observation of Foamy Slag through Transparent Quartz Windows

Transparent quartz windows were installed in the interior smelter wall to observe the various physical and chemical processes occurring within the foamy slag. The optimum installation point would be at or below the foamy slag level. The windows were installed well above the slag line due to the obvious concerns with cracking and breakout. This location provided detailed information on conditions inside the smelter during oxygen blowing.

Windows of various diameters and thickness were obtained. Initially a 4½" window was installed on the sampling port at the top of the smelter to test its viability. Three trials were run with larger windows installed in the sidewall at the north end of the smelter. A water-cooled door was designed which allowed installation of a small window on the outside of the shell and a larger diameter window on the inside of the shell. This arrangement prevented leakage of furnace slag or gases in the event of the inside window failing. A video camera was used to record various events inside the furnace.

The quartz windows survived the high temperature environment very well. In the first heat, H-19, the window lasted for about one hour before falling into the bath due to melting of the cement compound on the window edges. The window became almost opaque with slag-metal splash which froze and did not melt away. When the inside window fell off, small metal droplets, ≈ ¼" diameter, and char particles, ¼" to ½", were observed to fly into the window tunnel. Extremely bright flashes were seen in the gas phase indicating high temperatures from postcombustion.

In the second heat, H-20, the window quickly became coated with slag-metal splash and was rendered semi-transparent. In the third heat, H-21, the window lasted for about 4½ hours. Again, small slag-metal drops as well as large slag drops, 1" - 2" size, were seen splashing in the window area. Bright flashes were observed in the background indicating post-combustion reactions. After the inside window cracked and melted, pulsating foamy slag and high temperature bright areas with char particles were clearly seen in the furnace.

The quartz window experiments provided useful information on the state of the smelter interior during oxygen blowing. The window could be used as a predictive tool in future smelter installations. High speed videos can be used to measure and define the movement of metal, slag, char, and ore particles.

Oxygen Blowing Practice in the Smelter

Experimental data from the vertical and horizontal smelter trials were evaluated and recommendations formulated for the oxygen blowing practice. The main oxygen lance design was specified in terms of orientation, velocity, and number of primary and secondary oxygen jets. Two sets of lance designs were specified: a two lance "Soft Blow" configuration for maximizing postcombustion and a three lance "Hard Blow" configuration to optimize jet penetration and stirring in the foamy slag. A measure of effectiveness was developed based on the PCD (postcombustion degree) and "oxygen split ratio", reaction of oxygen with the gas or liquid/solid. These measures allowed quantitative analysis for the performance of the oxygen lance designs. The PCD was effectively controlled between 20 to 40%.

A carbon balance predictive model was formulated and used during the last four two-zone smelter trials. This model was based on a three point weighted average for the last three values of carbon transfer between backmixing and char and dust pickup in the steelmaking zone. The model was used to generate values for the next control point. Agreement between predicted and measured carbon was good.